



Pergamon

Journal of the Mechanics and Physics of Solids  
48 (2000) 2467–2512

---

---

JOURNAL OF THE  
MECHANICS AND  
PHYSICS OF SOLIDS

---

---

www.elsevier.com/locate/jmps

# An extended model for void growth and coalescence

T. Pardoen<sup>a, b,\*</sup>, J.W. Hutchinson<sup>a</sup>

<sup>a</sup> *Division of Engineering and Applied Sciences, Harvard University, Pierce Hall, Cambridge, MA 02138, USA*

<sup>b</sup> *Département des Sciences des Matériaux et des Procédés, Université catholique de Louvain, PCIM, Place Sainte Barbe 2, B-1348 Louvain-la-Neuve, Belgium*

Received 12 October 1999; received in revised form 21 February 2000

---

## Abstract

A model for the axisymmetric growth and coalescence of small internal voids in elastoplastic solids is proposed and assessed using void cell computations. Two contributions existing in the literature have been integrated into the enhanced model. The first is the model of Gologanu–Leblond–Devaux, extending the Gurson model to void shape effects. The second is the approach of Thomason for the onset of void coalescence. Each of these has been extended heuristically to account for strain hardening. In addition, a micromechanically-based simple constitutive model for the void coalescence stage is proposed to supplement the criterion for the onset of coalescence. The fully enhanced Gurson model depends on the flow properties of the material and the dimensional ratios of the void-cell representative volume element. Phenomenological parameters such as critical porosities are not employed in the enhanced model. It incorporates the effect of void shape, relative void spacing, strain hardening, and porosity. The effect of the relative void spacing on void coalescence, which has not yet been carefully addressed in the literature, has received special attention. Using cell model computations, accurate predictions through final fracture have been obtained for a wide range of porosity, void spacing, initial void shape, strain hardening, and stress triaxiality. These predictions have been used to assess the enhanced model. © 2000 Elsevier Science Ltd. All rights reserved.

*Keywords:* A. Fracture mechanisms; A. Voids and inclusions; B. Constitutive behavior; B. Elastic-plastic porous material; C. Finite elements

---

---

\* Corresponding author. Fax: +1-617-495-9837.  
E-mail address: pardoen@pcim.ucl.ac.be (T. Pardoen).

## 1. Introduction

### 1.1. Preliminaries

Recent efforts in the development of computational models incorporating the void growth process has given rise to robust predictive methods for crack propagation in ductile solids (e.g. Needleman and Tvergaard, 1987; Rousselier et al., 1989; Mudry et al., 1989; Bethmont et al., 1990; Bilby et al., 1993; Xia et al., 1995; Xia and Shih, 1995a,b; Brocks et al., 1995a; Ruggieri et al., 1996; Gao et al., 1998). Most strikingly, the strong geometry dependence of crack growth resistance curves emerges without the introduction of phenomenological parameters for the characterization of crack tip constraint. Most of these works employed the constitutive model initially proposed by Gurson (1977), improved by Tvergaard (1981, 1982), and finally extended by Needleman and Tvergaard (1984) to account for the rapid loss of load carrying capacity during void coalescence. It has also been supplemented by various kinds of void nucleation criteria (e.g. Chu and Needleman, 1980; Saje et al., 1982; Pineau, 1992). Although good agreement with a range of experiments and void cell computations has been observed, the model as it currently stands still suffers from significant limitations:

- The transfer of experimental data obtained from non-cracked specimens for the modeling of cracked structures, and vice versa, is not yet successful. In order to quantitatively reproduce experimental  $J_R$  curves, parameters of the model must be identified by fitting to test data taken under high stress triaxiality conditions such as from a cracked specimen (e.g. Gao et al., 1998). Many problems of ductile fracture in non-cracked structures occur at low to intermediate stress triaxiality, e.g. during metal forming processes like die-extrusion or in structures containing sharp or smooth notches. In such applications, the model does not reliably predict fracture using a set of parameters identified at high triaxiality.
- In the context of the model as it now stands, non-spherical voids can only be accounted for in an ad hoc manner by introduction of an effective porosity. Even when cavities are initially spherical, void shape effects can be significant upon growth, especially at low stress triaxiality.
- The criteria currently employed to signal the void coalescence stage of deformation are limited to a restricted range of conditions, which are not easily measured experimentally. In particular, the significant stress triaxiality dependence of the coalescence condition is not captured by current models.

These limitations, and others, are thought to arise mainly because (i) *void shape* is not directly accounted for and (ii) *void coalescence* is not properly modeled. The objective of the present paper is to extend the Gurson model to include these effects and to assess the enhanced model to ascertain whether, in principle, it will be able to overcome the aforementioned limitations. To put the challenge in the simplest

terms, it is hoped that an extended void growth model can be developed which is capable of simultaneously providing accurate predictions for both *crack formation* prior to the existence of a crack and *crack growth* from pre-existing cracks. A successful extension along these lines would represent a major step towards attainment of a complete model for failure due to the ductile failure mechanism of void nucleation, growth and coalescence.

In extending the Gurson model it is inevitable that a more complicated model will emerge. Nevertheless, every effort has been made to retain the original structure of the model and to introduce a minimum of new parameters, mainly those which characterize void shape and relative spacing. It is recognized that the model is almost exclusively used in numerical computations, and thus certain modifications in the extended model, such as more complicated functional behaviors, will not necessarily cause any fundamental difficulty in its implementation. In the present work, we have borrowed heavily from two contributions existing in the literature, and have integrated them into the enhanced model. The first contribution is the model of Gologanu–Leblond–Devaux (Gologanu et al., 1995), extending the Gurson model to void shape effects. The second is the approach of Thomason (1990) for the onset of void coalescence. Each of these has been extended heuristically to account for strain hardening. In addition, a micromechanically-based simple constitutive model for the void coalescence stage is proposed to supplement the criterion for the onset of void coalescence. The various parts of the enhanced model are assessed using void cell computations. General discussion about void shape effects in elastoplastic or viscoplastic materials can be found elsewhere (e.g. Budiansky et al., 1982; Lee and Mear, 1992; Gologanu et al., 1995; Sovik and Thaulow, 1997; Benzerga et al., 1999). Emphasis will be put in this paper on some of the details of void coalescence because they are less well understood.

## 1.2. Organization of the paper

Since there is a multitude of aspects in this enhanced model, reflected in the parameters of the void growth/coalescence model, a synoptic overview of the full model will be presented in the Introduction following some background about the coalescence of voids. The synopsis will be limited to a schematic description of the main equations of the model without details of the explicit forms for the equations, which are contained in the body and Appendix A of the paper. Following the Introduction, the paper begins by describing the phenomenology of tensile void coalescence from results obtained using void cell computations. Then, the coalescence model is presented and assessed. The fully enhanced model follows.

The sections are organized as follows: Section 2, Computational void cell model; Section 3, Void cell results; Section 4, Void coalescence model; Section 5, Analysis of the full model for void growth and coalescence; Section 6, Conclusions and perspectives; Appendix A, details of the equations of the void growth model.

### 1.3. Background about void coalescence

Void coalescence is the final stage in the failure mode of ductile materials. It consists in the localization of plastic deformation at the microscale inside the intervoid ligament between neighboring voids, with material off the localization plane usually undergoing elastic unloading. Localization can occur at any orientation relative to the principal straining axis, depending on the orientation of the ligament between the two coalescing voids: tensile (i.e. normal separations) or shear localizations are possible.

The *tensile void coalescence* mechanism implies a transition to a uniaxial straining mode of the representative volume element, as shown by Koplik and Needleman (1988). It is a diffuse localization at the microscale. Experimentally, the tensile coalescence mode brings about the flat dimpled fracture morphology widely observed in an enormous range of ductile materials under a wide range of stress states. After the onset of void coalescence, voids grow rapidly until final impingement. To establish precise terminology, in this paper “void coalescence” has been reserved for the part of the void enlargement evolution after the transition to the uniaxial straining mode, and “void growth” is used to characterize void enlargement before localization. “*Shear*” *coalescence* (e.g. Tvergaard, 1981; Faleskog and Shih, 1997) is favored by low stress triaxiality, low strain biaxiality and low strain-hardening. This mode of coalescence is similar to shear banding but at the scale of the voids. Overall axisymmetric deformations bring about a kinematic constraint, which tends to exclude localization in shear bands.

In practice, the nucleation and rapid growth of a second population of smaller voids inside the intervoid ligament has been observed in several steels and aluminum alloys (Rogers, 1960; Cox and Low, 1974; Hancock and Mackenzie, 1977; Achon, 1994) and is recognized to precipitate ligament failure (Tvergaard, 1981; Brocks et al., 1995b; Faleskog and Shih, 1997) well before impingement of the large voids. When a second, smaller population of voids intervenes, the coalescence mechanism is called a “void sheet”.

The void coalescence mechanism is a localization mechanism at the scale of the void size that must thus be distinguished from the localization in a band at the “mesoscopic” scale with a width typically of the order of one or more void spacings (e.g. Tvergaard, 1981). The confusion can arise because of the fact that when such a mesoscopic localized band develops, coalescence usually follows soon after leading to fracture with a small additional increase in remote displacements. Inside the band, the cavities grow very rapidly due to the large mesoscopic strain rates. Void coalescence, in the sense defined here, follows the onset of the mesoscopic plastic localization when one occurs. For practical purposes, mesoscopic localization can be regarded as the onset of fracture, even though the distinct micromechanism of coalescence will develop somewhat later within the band.

Modeling of void coalescence has received far less attention in the literature than void growth. The most widely employed criterion for the onset of void coalescence states that void coalescence starts at a critical porosity which has tended to be regarded as a material constant (McClintock, 1968b; d’Escatha and Devaux, 1979).

Several numerical (e.g. Koplik and Needleman, 1988; Tvergaard, 1990; Brocks et al., 1995b) and experimental/numerical works (e.g. Marini et al., 1985; Becker, 1987; Pardoen et al., 1998) have assessed the validity of this attractive but overly simplified fracture criterion. For a well defined material (and microstructure) and a fairly limited range of thermomechanical loading, this criterion appears to be acceptable from a practical standpoint. However, it will be demonstrated that any general void coalescence model requires the introduction of at least some microstructural information related to the void/ligament dimensions and geometry. This fact was recognized by McClintock (1968b) in his original study and has been discussed in detail by Thomason (1990, 1993).

#### 1.4. Synopsis of the model

The parameters characterizing a representative volume element (RVE) are defined in Fig. 1. Throughout the paper, subscripts “0” and “c” indicate initial values and values at the onset of void coalescence, respectively. The extension of the Gurson model due to Gologanu et al. (1995), which has been adopted here to describe behavior prior to void coalescence, gives a constitutive relation for a porous elastoplastic material containing (axisymmetric) spheroidal voids. This particular model, extended for strain-hardening, contains nine state variables: the six components of the mesoscopic stress tensor,  $\Sigma$ , the porosity,  $f$ , the void aspect ratio,  $S$ , and an average yield stress for the matrix material,  $\sigma_m$ . The void aspect ratio is defined by  $S=\ln(W)$  while  $W=R_z/R_r$ . The functional form of model prior to coalescence is:

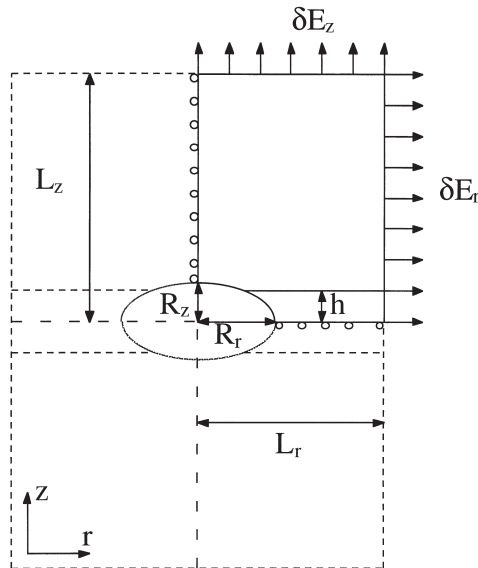


Fig. 1. Representative volume element, with the geometric parameters, symmetry lines, and boundary conditions.

$$\Phi \equiv \Phi(\Sigma, f, S, \sigma_m) = 0, \tag{1}$$

$$\dot{f} = (1-f)\dot{E}^p_{kk}, \tag{2}$$

$$\dot{S} \equiv \dot{S}(f, S, T), \tag{3}$$

$$\sigma_m \dot{\epsilon}^p_m (1-f) = \Sigma_{ij} \dot{E}^p_{ij}, \tag{4}$$

$$\sigma_m \equiv \sigma_m(\epsilon_m), \tag{5}$$

$$\dot{E}^p_{ij} = \gamma \frac{d\Phi}{d\Sigma_{ij}}, \tag{6}$$

where  $\Phi$  is the flow potential;  $E^p$  is the mesoscopic plastic strain tensor; (2) and (3) are the evolution laws for  $f$  and  $S$ , respectively, with  $T$  being a stress triaxiality measure defined as the ratio of the hydrostatic stress by the effective stress,  $\Sigma_h/\Sigma_e$ ; (4) is the simple Gurson (1977) energy balance for the plastic work allowing computation of  $\sigma_m$  using the effective stress–strain curve for the parent material (5); and (6) is the flow rule. As already emphasized, the structure of the original Gurson model has been retained. Explicit expressions for the functions such as  $\Phi$  and  $\dot{S}$  will be given elsewhere in the paper.

A criterion for the onset of tensile localization in the ligaments between the voids is obtained in the spirit of Thomason’s approach (1990). This criterion requires the introduction of an additional variable,  $A$ , characterizing the void distribution and defined as  $A = \ln(L_z/L_r)$  (see Fig. 1). Its evolution law is simply

$$\dot{A} = \dot{E}_z - \dot{E}_r. \tag{7}$$

The criterion for the onset of void coalescence is a function of the current RVE geometry and hardening of the matrix material with the general form

$$\frac{\Sigma_z}{\sigma_0} = F_1\left(\frac{\sigma_m}{\sigma_0}, A, S, f\right). \tag{8}$$

This equation results from the condition that the applied stress component normal to the localization plane (left-hand side) must give rise to an average mean tensile stress in the intervoid ligament allowing the transition to a localized yielding mode in the current RVE geometry. The evolution of the mesoscopic stress after the onset of coalescence is then determined by the localization process. Localization brings about uniaxial straining of the RVE which permits simple expressions to be derived for the evolution of  $\sigma_m$ ,  $A$ ,  $f$  and  $S$  during void coalescence (see Section 4.2). The evolution of the stress continues to be expressed as (8), and  $f$  and  $A$  are still derived from the incompressibility rule (2) and Eq. (7) (with  $\dot{E}_r = 0$  if elasticity is neglected), respectively. Eq. (4) ceases to be relevant after the onset of coalescence, and the evolution of  $\sigma_m$  is deduced from an approximate equation for the average effective strain rate in the localized band,  $\dot{\epsilon}^{loc}_e$ , and the uniaxial flow properties of the sound material (5):

$$\dot{\epsilon}^{loc}_e = F_2(f, S, A)\dot{E}_z. \tag{9}$$

Finally,  $\dot{S}$  is determined from

$$\dot{S} = \frac{3}{2} F_3(f, a, S) \dot{E}_z. \tag{10}$$

The functions  $F_1$ ,  $F_2$  and  $F_3$  are derived in Sections 4.1 and 4.2.

Table 1 gathers the material and “tuning” parameters (the  $q$  factor) which must be specified in the model.

Table 1

Comparison between the version of the Gurson model enhanced by Needleman and Tvergaard (1984) and the version of the model proposed in the present paper. The comparison is made in terms of the parameters of both models

|                          | (A) Gurson model enhanced by Tvergaard and Needleman | (B) New model   | Comments   |
|--------------------------|--|---|--|
| Flow properties          |  | $\sigma_0, E, n, \nu$   |  |
| Microstructural features |  | $f_0$   | $f_0$ in (A) is an effective porosity when used to model non-spherical voids   |
|                          | $L_0$  | $S_0 = \ln(R_{z0}/R_{r0})$<br>$\lambda_0 = L_{z0}/L_{r0}$<br>$L_{r0}$                               | When used to model crack propagation, both models will require a material length: in principle, the void spacing. Adjusting this length is the simplest way to account for heterogeneous void distributions  |
| Void nucleation          |  | Not addressed in this work; existing nucleation models could identically be applied with (A) or (B) |  |
| Void growth              | $q$ (or $q_1$ ), $(q_2)$                             | $q$   | An heuristic parameter $q$ is required in both models to accurately predict the void growth rates. It is generally a function of $n, f_0, T$ and $S$ , determined from cell computations. In (A), a second parameter $q_2$ is sometimes introduced to account for the void shape |
| Void coalescence         | $f_c, f_E$   |   | The critical porosities in (A) depend on the stress triaxiality, on the microstructure ( $f_0, \dots$ ), and on the flow properties  |

## 2. Computational void cell model

The void cell method (Needleman, 1972) is revisited in order to address in a comprehensive way the effect of initial porosity, strain hardening exponent, stress triaxiality, void shape, and void distribution on void coalescence. Following earlier efforts, the continuum analyzed in the present work is imagined as a periodic array of hexagonal cylindrical unit cells, each containing an aligned spheroidal void. For the sake of simplicity, this assemblage is approximated by circular cylinders allowing axisymmetric calculations which have been shown to provide a good approximation to the hexagonal cells (e.g. Worswick and Pick, 1990). More complex assemblages or stress states have been analyzed by several authors (e.g. for 3D computations, Hom and McMeeking, 1989; Richelsen and Tvergaard, 1994; Kuna and Sun, 1996; Thomson et al., 1999). A cell is characterized by three parameters: the initial porosity,  $f_0$ , the initial aspect ratio of the void,  $W_0$ , and the initial aspect ratio of the cell,  $\lambda_0$ . These parameters are defined from the characteristic dimensions of the void cell in Fig. 1 as:

$$f_0 = \frac{2R_{r0}^2 R_{z0}}{3L_{r0}^2 L_{z0}}, \quad (11)$$

$$W_0 = \exp(S_0) = \frac{R_{z0}}{R_{r0}}, \quad (12)$$

$$\lambda_0 = \exp(A_0) = \frac{L_{z0}}{L_{r0}}, \quad (13)$$

where  $R_{r0}$ ,  $R_{z0}$ ,  $L_{r0}$ ,  $L_{z0}$  are the radial and axial half-lengths of the spheroidal void and cell, respectively. The parameters  $S$  and  $W$  will be called “aspect ratio” or “void shape” for short. The two limiting cases,  $W \rightarrow 0$  and  $W \rightarrow \infty$  correspond, when the porosity goes to zero, to the penny-shape crack and the infinitely thin needle, respectively, and, when the porosity is kept constant, to a “sandwich” and the infinitely long hollow cylinder, respectively.

The mesoscopic principal strains and a special “effective” strain measure are given by

$$E_r = \ln\left(\frac{L_r}{L_{r0}}\right); E_z = \ln\left(\frac{L_z}{L_{z0}}\right); E_e = \frac{2}{3}|E_z - E_r|. \quad (14)$$

The mesoscopic true principal stresses are the average forces at the cell boundary per current area. The effective stress and hydrostatic stress are

$$\Sigma_e = |\Sigma_z - \Sigma_r|; \Sigma_h = \frac{1}{3}(\Sigma_z + 2\Sigma_r). \quad (15)$$

The current porosity  $f$  is computed via the condition of plastic incompressibility of the material surrounding the void. Based on the approximation of Koplik and Needleman (1988) for the elastic dilatation, one has

$$f = 1 - (1 - f_0) \frac{V_0}{V} \left( 1 + \frac{3(1 - 2\nu)}{E} \Sigma_h \right), \tag{16}$$

where  $V_0$  and  $V$  are the initial and current volume of the cell, respectively;  $\nu$  is the Poisson ratio and  $E$  is the Young's modulus of the matrix material.

The computations were performed within the finite strain setting using the general-purpose finite element program ABAQUS Version 5.7 (1997). Computations have been carried out at a prescribed fixed triaxiality,. Several methods can be used to impose constant stress triaxiality on the cell. In the present work, a constant axial increment of displacement is prescribed while the radial increment is adjusted using an iterative method until the desired  $T$  is attained. Axisymmetric nine-node isoparametric elements with reduced integration were chosen. As shown in Fig. 2, the mesh was highly refined close to the void surface with nearly flat elements to preserve a reasonable aspect ratio for these elements when deformed to very large strains. Convergence analyses were systematically performed by examining the effect of both mesh refinement and smaller applied displacement increments. Convergence was considered as being attained when no change in the strain at the onset of void coalescence was observed. After the onset of void coalescence the effective stress drops rapidly due to localization in the ligament. The validity of the numerical results is expected to rapidly deteriorate after the onset of void coalescence because of mesh distortion. However, convergence was observed for a portion of the  $\Sigma_e - E_e$  curve after the onset of void coalescence. It is worth mentioning that the region in which

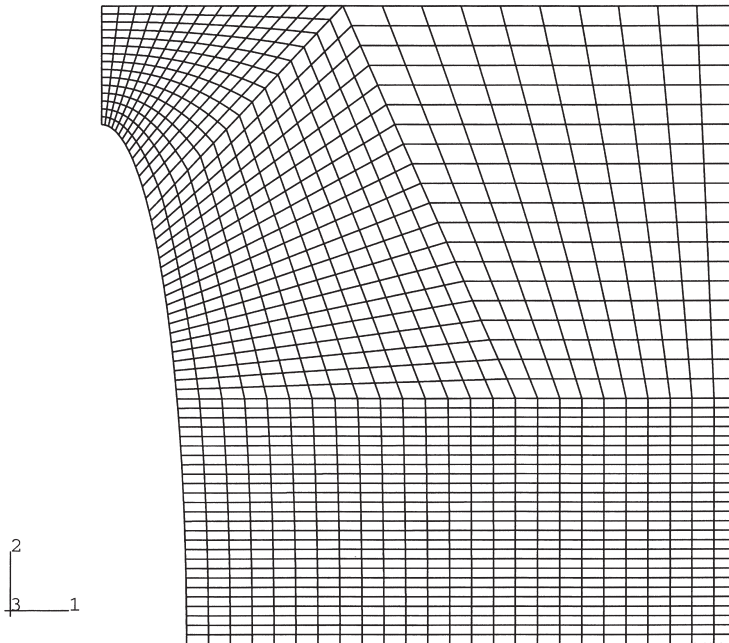


Fig. 2. Finite element mesh for an initially prolate void ( $W_0=6$ ) in 1:1 cell ( $\lambda_0=1$ ).

plastic deformations localize during void coalescence is not restricted to a single row of elements located in the minimum section of the intervoid ligament. When the mesh is sufficiently refined, localization is diffusely spread over several rows of elements. Thus, intrinsic mesh sensitivity did not affect the present results.

The constitutive behavior of the matrix material is the rate independent  $J_2$  elastoplastic model. The specific uniaxial true stress–true strain curve is:

$$\frac{\sigma}{\sigma_0} = \frac{E\varepsilon}{\sigma_0} \text{ when } \sigma < \sigma_0, \quad (17a)$$

$$\frac{\sigma}{\sigma_0} = \left(1 + \frac{E\varepsilon^p}{\sigma_0}\right)^n \text{ when } \sigma > \sigma_0, \quad (17b)$$

where  $\sigma_0$  is the initial yield stress and  $n$  is the strain-hardening exponent.

The parameter choices used in the computations in this work are listed below, along with some comments as to their relevance. All possible combinations have not been investigated, and the parameters which have been addressed in only a limited number of void cell computations are included within parentheses.

- $f_0=10^{-4}$ ,  $10^{-2}$ ,  $(2 \times 10^{-2})$  and  $(6 \times 10^{-2})$ : a wide range of typical materials contain initial porosity between  $10^{-4}$  and  $10^{-2}$  (i.e. void volume fraction of potential nucleation sites as inclusions or precipitates). Nowadays, steels and aluminum alloys are processed having effective initial porosities well below  $10^{-4}$ , but even smaller porosity would require remeshing techniques to obtain results valid at the onset of void coalescence.
- $T=1/3$ ,  $(0.5)$ ,  $2/3$ ,  $1$ ,  $2$ ,  $3$ ,  $4$ ,  $(5)$ : this covers the range of stress states encountered in nearly all structural applications of interest here, from uniaxial tensile loading to high triaxiality crack tip fracture process zones.
- $n=0.1$  and  $0.3$ .
- $W_0=1/6$ ,  $1$ ,  $6$ : this range of parameters may seem quite large, but it is important to recall that in rolled steel plates, for example, MnS particles (the void nucleation sites) with aspect ratios larger than 20 can be found. Consideration of large and small aspect ratio clearly illuminates void shape effects. Numerical analyses of aspect ratios larger than 6 or smaller than  $1/6$  are more complex and less accurate because of the marked strain gradients which develop at the regions of high curvature of the void surface.
- $\lambda_0=(1/2)$ ,  $1$ ,  $(2)$ ,  $4$ ,  $(6)$ ,  $(8)$ ,  $16$ .
- $\sigma_0/E=0.002$ : this parameter plays a secondary role in the phenomena of interest.

### 3. Void cell results

#### 3.1. Role of the primary parameters

This presentation focuses on void coalescence. Specific considerations regarding the effect of the void shape on the void growth phase for initially non-spherical

voids can be found in recent papers by Gologanu et al. (1993, 1994, 1995) and Sovik and Thaulow (1997).

### 3.1.1. Influence of $W_0$ and $T$

Fig. 3(a–d) gathers results for the entire process from the void growth stage through void coalescence in a material with  $n=0.1$ ,  $f_0=10^{-2}$ , and  $\lambda_0=1$ . Three stress triaxialities and three initial void shapes are considered:  $T=1/3$ , 1 and 3 and  $W_0=1/6$ , 1, and 6. Fig. 3(a) displays variations of the axial stress  $\Sigma_z$  as a function of the axial strain  $E_z$ . The onset of void coalescence corresponds to a marked change of the slope of the curves. The transition is most sharp at low stress triaxiality. The effect of void shape is very marked at low stress triaxiality. Coalescence is observed in uniaxial tension, i.e.  $T=1/3$ , for initially oblate voids ( $W_0=1/6$ ), but no void coalescence is observed for  $W_0=1$  and 6. The void shape effect on the onset of coalescence is still pronounced at  $T=1$ , but decreases with increasing stress triaxiality. After the onset of void coalescence the falling stress–strain curve is nearly linear, except after the voids have become so large that the validity of the numerics begins to deteriorate. In an analysis using remeshing techniques for extreme void expansion at an interface between a metal and a ceramic, Tvergaard (1997) has shown that the overall stress drop remains linear until the load becomes nearly zero.

Fig. 3(b, c) exhibits the variations of, respectively,  $f$  and  $S=\ln(W)$  as a function of  $E_z$ . The effect of stress triaxiality on the rates of  $f$  and  $W$  has been well covered in the literature (e.g. McClintock, 1968a; Budiansky et al., 1982; Koplik and Needleman, 1988; Gologanu et al., 1995). Void coalescence induces an increase in the void growth rate and a transition in the void shape evolution. After the onset of void coalescence, the radial growth is significantly larger than the axial growth (except for the case  $W_0=1/6$  at  $T=3$ ). The end of the coalescence process in a real material usually consists of the failure of the remaining ligament (by microcleavage, crystallographic shearing, or with the help of second population of smaller voids) rather than radial void growth until impingement. Thus, after the onset of void coalescence, the void expands rapidly in the radial direction until the final failure of the ligament. During this process, axial void growth remains small. Consequently,  $R_z$  measured on the fracture profile is a good approximation of the void half-height at the onset of void coalescence. *The most pertinent dimension to measure on a fracture profile to gain information about void coalescence is  $R_z$ .*

Fig. 3(d) shows the variation in the radial strain  $E_r$  as a function of the axial strain  $E_z$ . The transition to a uniaxial straining mode is nearly always essentially instantaneous (see also Koplik and Needleman, 1988; Becker et al., 1989 for initially oblate voids, Brocks et al., 1995b, and Richelsen and Tvergaard (1994) for 3D computations). This transition constitutes a direct indicator of localization and is effective in quantifying the strain at the onset of void coalescence. Exceptionally, at high stress triaxiality and for highly elongated cells ( $\lambda \gg 1$ ) (not shown in Fig. 3(d)), the transition is not so marked due to elastic effects on  $E_r$ . In that case, accurate detection of the transition to localization requires examination of the radial strain rate variation as a function of  $E_z$ .

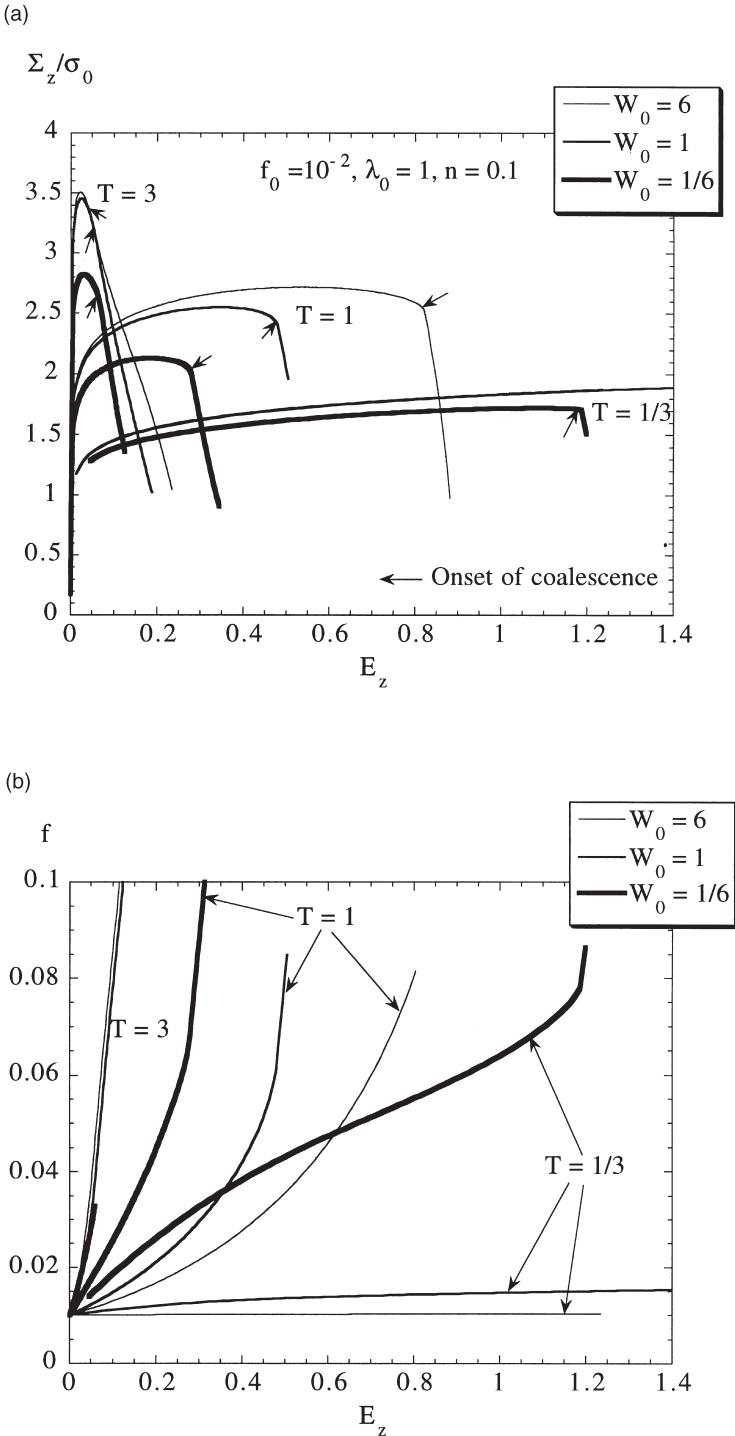
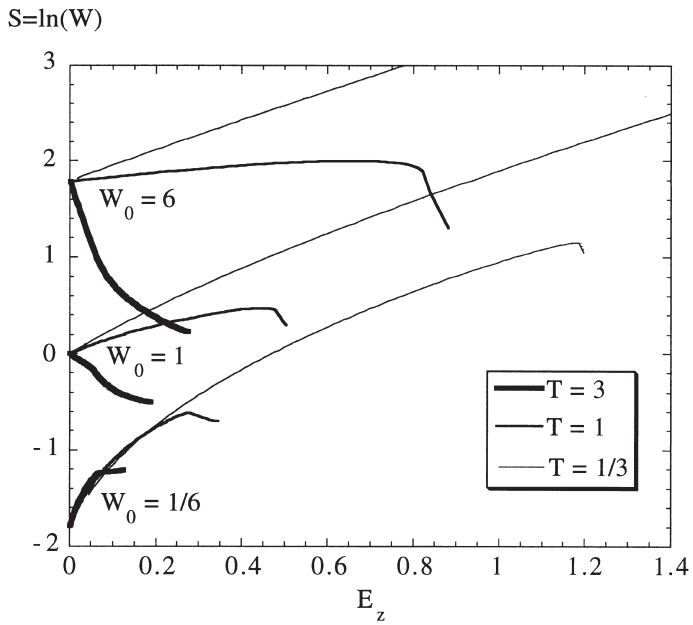


Fig. 3. Void cell results for  $f_0=10^{-2}$ ,  $\lambda_0=1$ ,  $\sigma_0/E=0.002$ ,  $n=0.1$  and  $W_0=1/6, 1, 6$ , at  $T=1/3, 1, 3$ ; (a) (true) axial stress vs (true) axial strain; (b) porosity vs axial strain; (c) void shape vs axial strain; (d) true radial strain vs axial strain.

(c)



(d)

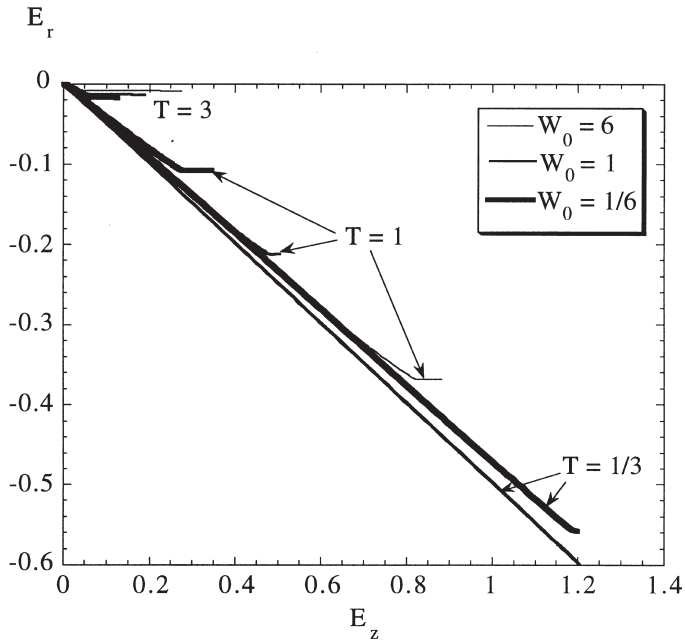


Fig. 3. (continued)

3.1.2. Influence of  $f_0$  and  $n$

Although quantitative differences in the predictions were observed for a material with  $n=0.3$  or  $f_0=10^{-4}$ , the general trends due to variations in  $T$  and  $W_0$  are similar to those just discussed. A selection of these results will be presented in the last section of the paper. Larger ductilities are predicted for decreasing  $f_0$  or increasing  $n$ . The most striking difference is the following: when  $n=0.1$  and  $f_0=10^{-4}$ , no void coalescence is observed for the initially oblate void ( $W_0=1/6$ ) at  $T=1/3$ , whereas it is observed for  $f_0=10^{-2}$  (see Fig. 3). The increase in porosity is found to arrest when  $f \approx 6 \times 10^{-4}$  (for  $f_0=10^{-4}$ ).

3.1.3. Influence of the void distribution

Fig. 4 summarizes the effects of the various geometrical parameters on void coalescence by gathering results for the following void cells: (1)  $f_0=10^{-2}$ ,  $W_0=1$ ,  $\lambda_0=1$ ; (2)  $f_0=10^{-2}$ ,  $W_0=1/6$ ,  $\lambda_0=1$ ; (3)  $f_0=6 \times 10^{-2}$ ,  $W_0=1$ ,  $\lambda_0=1$ ; (4)  $f_0=10^{-2}$ ,  $W_0=1$ ,  $\lambda_0=6$ . The cells were chosen such that the parameter  $L_{x0}/R_{x0}$ , which measures the relative radial void spacing, is equal to the same value 2.2 in cells (2), (3), and (4)

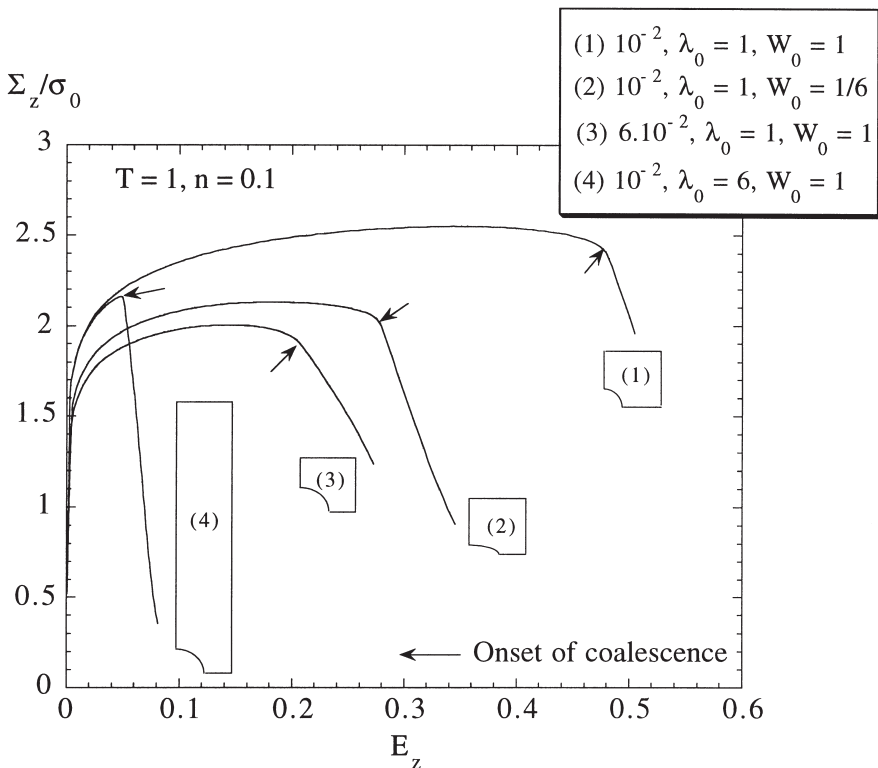


Fig. 4. Four void cell results for a stress triaxiality equal to 1 and  $n=0.1$ , displaying the effects of void shape, porosity, and void spacing.

whereas it is equal to 4.05 in cell (1). All the cells were loaded with a prescribed triaxiality  $T=1$ . Several comments can be made concerning the void coalescence:

- (i) The onset of void coalescence depends strongly on relative void spacing as can be discerned by comparing cells (1) and (4), which have identical void shapes and initial porosity. The effect can be seen in another way by comparing cells (2) and (3), which have been chosen with roughly similar void spacing: the cells have roughly similar coalescence strains, even though the initial void volume fractions and shapes are very different. The conclusion to be drawn is that heterogeneity in the void distribution inherited from prior working or processing plays a major role in the fracture resistance. This specific aspect of void distribution has already been investigated by several authors (e.g. Bourcier et al., 1986; Becker, 1987; Dubensky and Koss, 1987; Magnusen et al. 1988, 1990; Needleman and Kushner, 1990; Huang, 1993; Becker and Smelser, 1994; Leblond and Perrin, 1999; Thomson et al., 1999), although in most instances within the context of porosity-induced mesoscopic plastic localization, and not void coalescence.
- (ii) Void spacing is not the only influential parameter as can be seen when comparing cells (4) and (3) or (4) and (2). In these two comparisons, a higher level of mean stress builds up in the ligament of cell (4) accelerating localization.
- (iii) Very elongated cells (4) have steeper unloading curves due to the contribution from elastic unloading in the zone outside the ligament. For a similar cell aspect ratio, cells (2) and (3) also have significant differences between the slopes after the onset of void coalescence, in this case due to differing initial porosity and void shape.

As the effects of cell aspect ratio and void spacing have not received much attention in the literature (except for a few results by Koplik and Needleman, 1988; Tvergaard, 1998), some systematic trends are revealed in Figs. 5 and 6 and commented on in the next section.

### 3.2. Influences of the cell geometry

The effect of the initial cell aspect ratio  $\lambda_0$  on void coalescence is depicted in Fig. 5(a), which presents  $\Sigma_e$  vs  $E_e$  for  $n=0.1$ ,  $W_0=1$ ,  $T=1$  and  $L_{r0}/R_{r0}$  fixed at 3.22. The true stress–true strain curve of the matrix material is also plotted ( $f_0=0$ ). The peak stresses converge to a well defined point on the curve corresponding to  $f_0=0$  as  $\lambda_0$  increases. For  $\lambda_0=16$ , there is nearly no departure from the curve  $f_0=0$  prior to localization. The limit,  $\lambda_0 \rightarrow \infty$ , corresponds to a single plane of voids in an infinite solid. The transition to a uniaxial straining mode is observed for all values of  $\lambda_0$ . For large  $\lambda_0$ , the onset of void coalescence coincides with the peak stress, which, consequently, is due to the onset of the void coalescence localization process and not due to the competition between the hardening of the matrix and the softening due to void

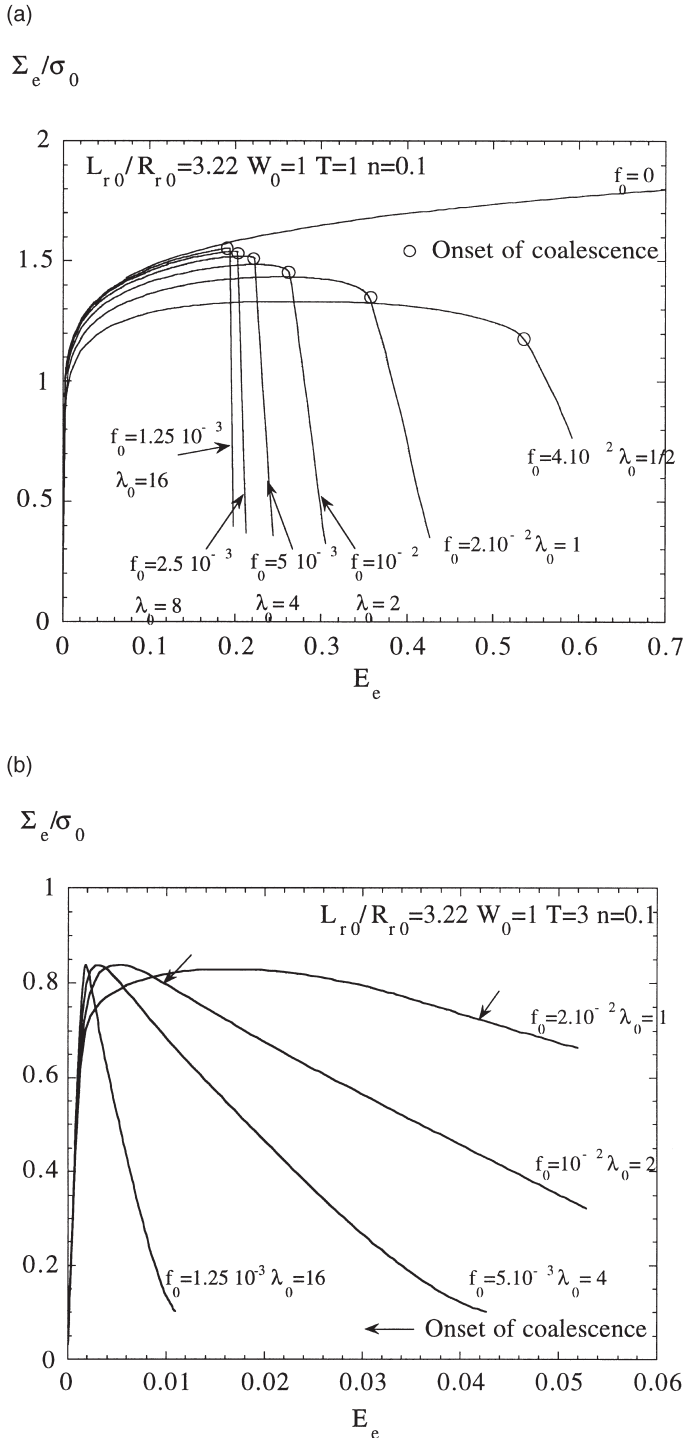


Fig. 5.  $\Sigma_z$  vs  $E_z$  curves for  $n=0.1$ ,  $W_0=1$ , a constant  $L_{r0}/R_{r0}$  ratio equal to 3.22, and  $T=1$  (a) or  $T=3$  (b), showing the effect of the cell aspect ratio (or, alternatively, of the porosity).

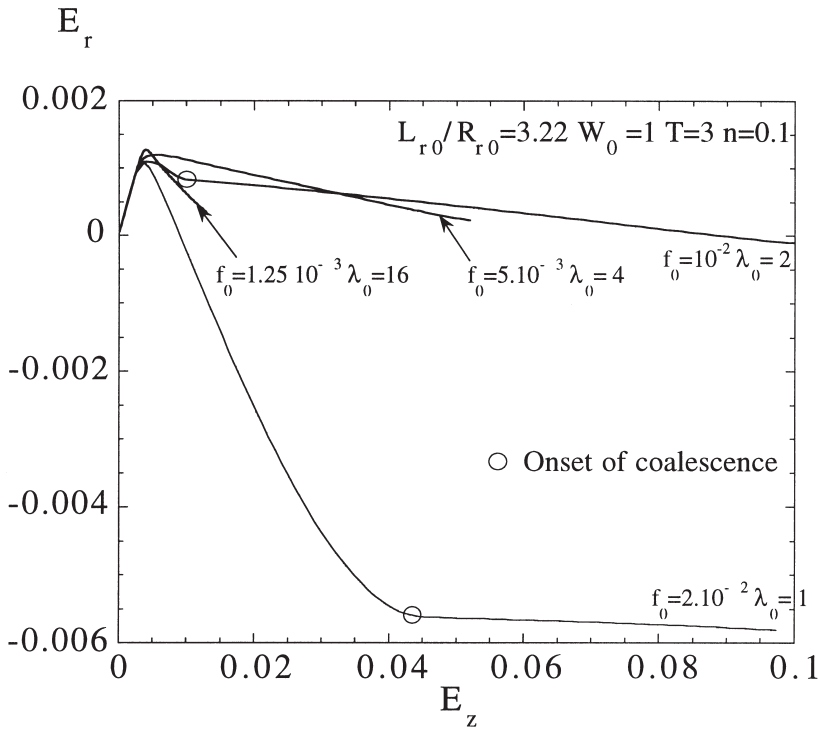


Fig. 6. Variations in the radial strain as a function of axial strain from void cells with identical void spacing, spherical voids,  $n=0.1$ , and  $T=3$ . The effect of the porosity, or, alternatively, of the cell aspect ratio, is very marked.

growth. The slope of the curve after the onset of coalescence increases with  $\lambda_0$  as a result of an increasingly larger zone of elastic unloading.

Fig. 5(b) presents analogous results for the case  $T=3$ , with all other parameters as before. Now, it is first interesting to note that in none of the void cells does the peak effective stress reach the yield stress of the matrix material. As for  $T=1$ , void coalescence imposes the attainment of the maximum stress when  $\lambda_0$  is increased. Furthermore, for  $\lambda_0=4$ , there is almost no plastic void growth prior to coalescence. The initial configuration and the stress triaxiality are such that localization in the intervoid ligament is favored over homogenous straining outside the ligament almost from the beginning of loading. Such a combination ( $T=3$ ,  $n=0.1$ ,  $f_0=5 \times 10^{-3}$ ,  $W_0=1$  and  $\lambda_0=4$ ) could correspond to the situation at a crack tip in a real material with an anisotropic initial distribution of inclusions. If the initial porosity is reduced, while maintaining  $\lambda_0 \geq 4$ , some plastic void growth again becomes necessary before the onset of coalescence. The variation in  $E_r$  corresponding to the results of Fig. 5(b) provides additional insights. Fig. 6 shows the variation in  $E_r$  as a function of  $E_z$  for  $T=3$ ,  $n=0.1$ ,  $W_0=1$ , and  $L_{r0}/R_{r0}$  fixed at 3.22. For  $\lambda_0 > 2$ , the transition in the radial strain rates  $\dot{E}_r$  is observed at coalescence, but is far from being equal to zero and remains significantly negative (a uniaxial straining mode is thus not observed). As a matter of fact, radial

elastic unloading of the cell becomes less and less negligible for increasing stress triaxiality, especially when  $\lambda_0$  increases. It is worth mentioning that the plastic part of  $\dot{E}_r$  is also not equal to zero implying that some reverse plasticity occurs.

Fig. 7 shows results for  $n=0.1$ ,  $W_0=1$ , and a constant  $\lambda_0=16$ , while  $L_{r0}/R_{r0}$  varies between 3.2 and 12.8, with Fig. 7(a) for  $T=1$  and Fig. 7(b) for  $T=3$ . These results isolate the effect of void spacing in the localization plane. Indeed, the void evolution is almost the same in each of the three cells (but different for the two triaxialities). The porosity is so low in each of these cases that the stress states are similar in the vicinity of the voids. Coalescence sets in abruptly and is a very strong function of  $L_{r0}/R_{r0}$  or, equivalently, of  $f_0$  given fixed  $\lambda_0$ , as well as the triaxiality  $T$ .

### 3.3. The RVE at the onset of void coalescence

The analysis of the stress and strain fields inside several void cells has shown that voids start interacting with each other well before the onset of void coalescence. Once localization of deformation within the ligament sets in, coalescence is fully underway. Fig. 8 depicts the differences observed between the localization zone during coalescence at low and large stress triaxiality. The height of the localization zone roughly corresponds to  $R_z$  at large stress triaxiality, while, at low stress triaxiality ( $T < 1-1.5$ ), it is only a fraction of  $R_z$ . Detailed analyses have shown that this fraction is fairly independent of the void shape for a given stress triaxiality.

Fig. 9(a) gathers the critical porosity of void cells characterized by  $n=0.1$ ,  $\lambda_0=1$  with  $f_0=10^{-2}$  or  $10^{-4}$  as a function of the stress triaxiality, for various  $W_0$  (1/6, 1, 6). As frequently mentioned in the literature (e.g. Koplik and Needleman, 1988; Brocks et al., 1995b; Pardoen et al., 1998), the critical porosity at the onset of coalescence significantly varies with  $T$ . These variations are such that a constant critical porosity is not an accurate criterion at low to intermediate stress triaxiality. However, at large stress triaxiality void growth rates are high enough before void coalescence such that the prediction of strain at coalescence based on a constant critical porosity may provide a reasonable approximation. The effect of  $T$  on  $f_c$  is not significantly more marked for initially prolate or oblate voids. The dependence of  $f_c$  on  $T$  varies with  $f_0$ : the maximum value of  $f_c$  is attained for smaller triaxialities when  $f_0$  increases (see also Benzerga et al., 1999). For large porosity ( $f_0=10^{-2}$ ), the value of  $f_c$  is influenced by the void shape at low stress triaxiality, whereas  $f_c$  for low porosity ( $f_0=10^{-4}$ ) is relatively independent of  $W$ . At  $T=5$ , a transition in the radial strain rate evolution becomes hardly detectable. For stress triaxiality larger than 5, unstable void growth has been found by several authors to be the central issue for the prediction of ductile failure (Ashby et al., 1989; Huang, 1991). Such high stress triaxiality is encountered only in very constrained problems, typically, a ductile thin metal layer between ceramic blocks (Tvergaard, 1991). Thus, for  $T > 5$  the distinction between void growth and void coalescence process becomes harder and harder to discern and the notion of critical porosity no longer meaningful.

For the same set of void cell parameters, Fig. 9(b) shows the critical values of the normalized radial radius of the void at the onset of void coalescence, denoted by  $R_{rc}/R_{r0}$ , where  $R_{r0}$  is the initial value. One might intuitively regard  $R_{rc}$  as a more

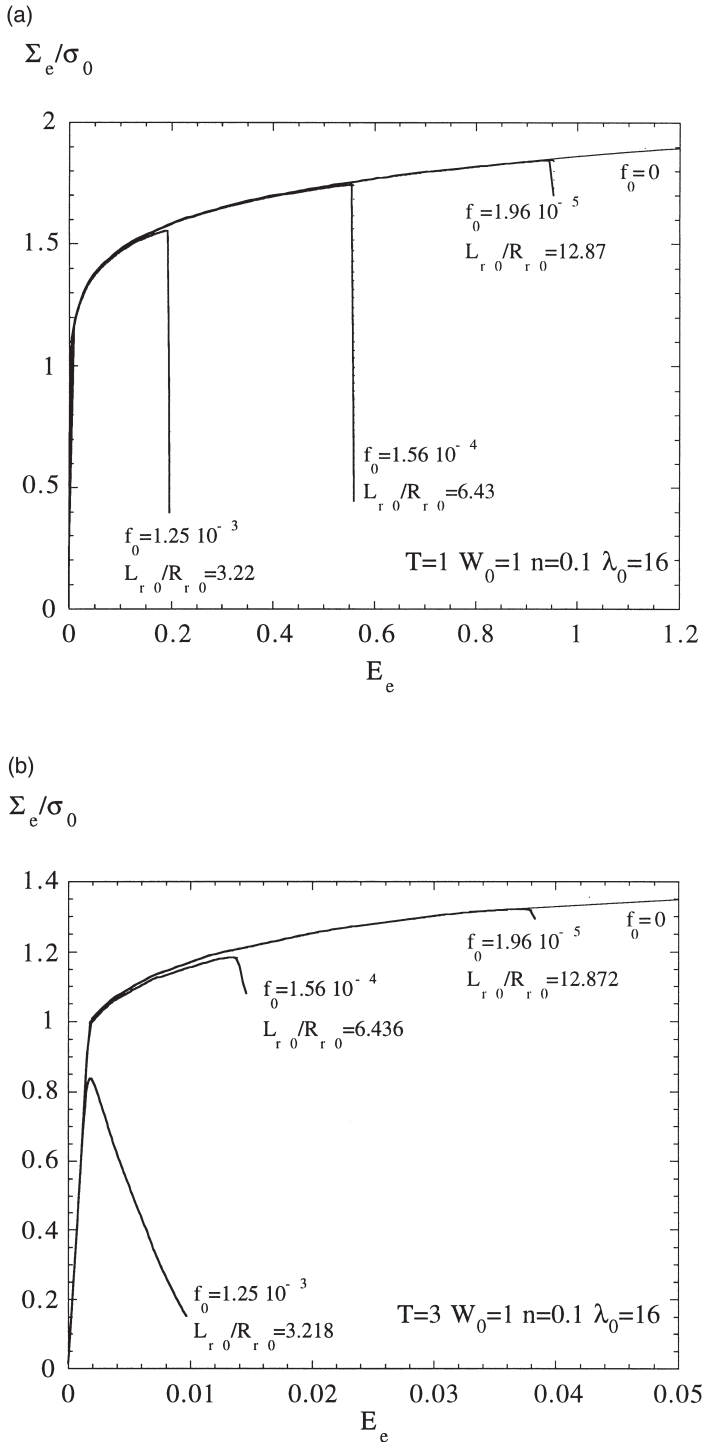


Fig. 7. Effective stress vs effective strain curves displaying the effect of the void spacing on elongated cells ( $\lambda_0=16$ ), for  $n=0.1$  and  $W_0=1$ ; (a)  $T=1$ ; (b)  $T=3$ .

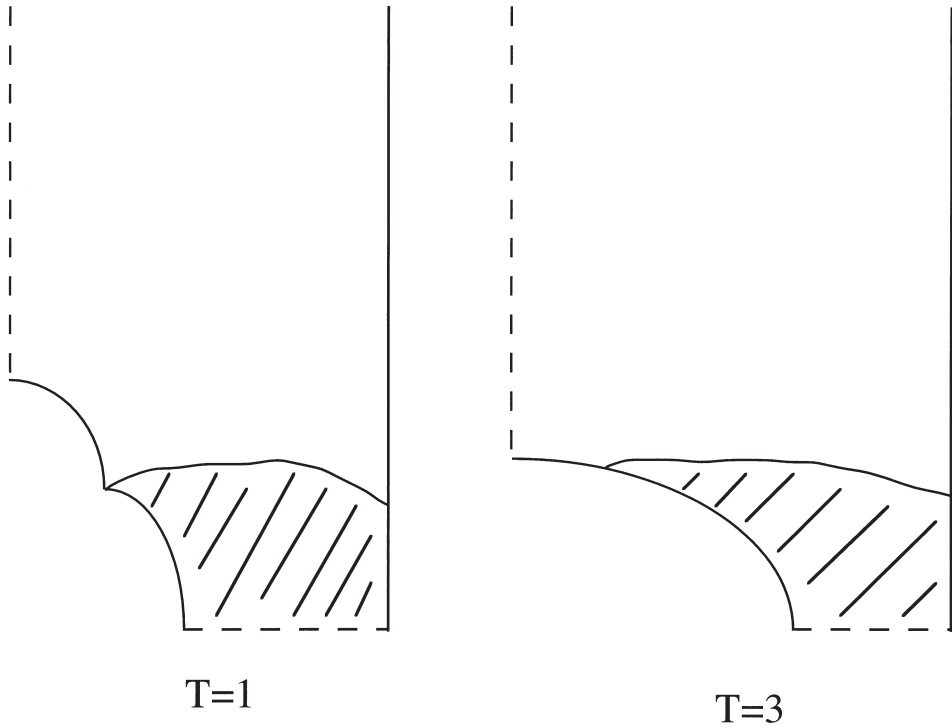


Fig. 8. Sketch of the zone of localized plastic straining during void coalescence, for two different stress triaxialities.

meaningful parameter for characterizing transverse void coalescence. However, Fig. 9(b) dispels that notion by virtue of the significant dependencies of  $R_{rc}$  on all of  $T$ ,  $f_0$  and  $W$ .

Fig. 10(a) compares the critical porosity  $f_c$  obtained for the two different strain-hardening exponents  $n=0.1$  and  $0.3$ , in all cases with  $f_0=10^{-2}$ . Except for low triaxiality, where the critical porosity depends only weakly on  $n$ , a larger strain-hardening exponent improves the resistance to the onset of void coalescence (i.e. larger  $f_c$ ) resulting in a larger equivalent strain at the onset of coalescence. Fig. 10(b) compares the  $R_{rc}/R_{r0}$  obtained for the two strain hardening exponents  $n=0.1$  and  $0.3$ ,  $f_0=10^{-2}$ .  $R_{rc}/R_{r0}$  lower than 1 at low stress triaxialities results from the void contraction. In real materials, the presence of a rigid inclusion can hinder this contraction resulting in a smaller void coalescence strain (e.g. Steglich and Brocks, 1997).

Fig. 11(a, b) shows the variations in  $f_c/f_0$  and  $W$  at void coalescence, respectively, as a function of  $\ln(\lambda_0)$ . They provide good estimates of the asymptotic values of  $f_c/f_0$  and  $W$  when  $\lambda_0 \rightarrow \infty$ , i.e. the limit when all the voids are confined to one plane.

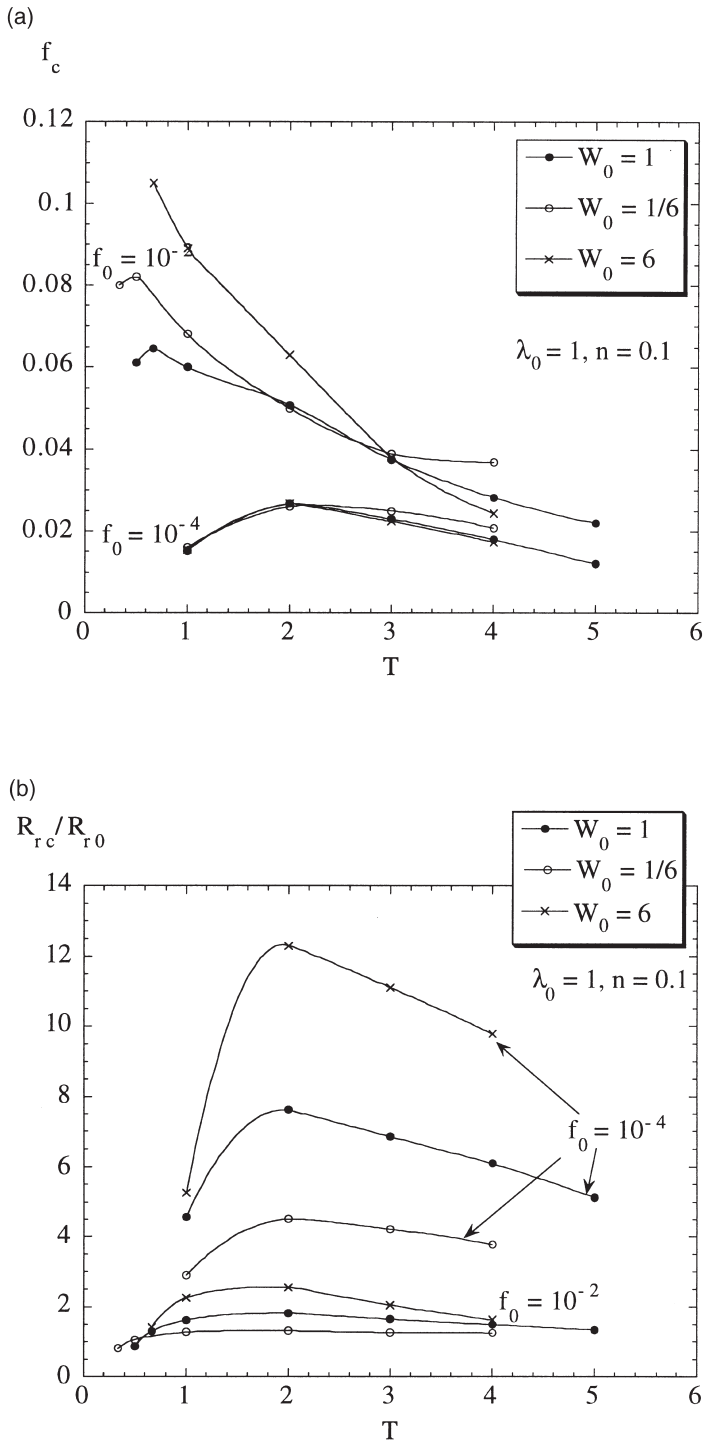


Fig. 9. Stress triaxiality dependence of critical damage parameters at the onset of coalescence, for different initial porosity and void shapes, with  $n=0.1$  and  $\lambda_0=1$ ; (a) critical porosity; (b) critical void radius (in the radial direction).

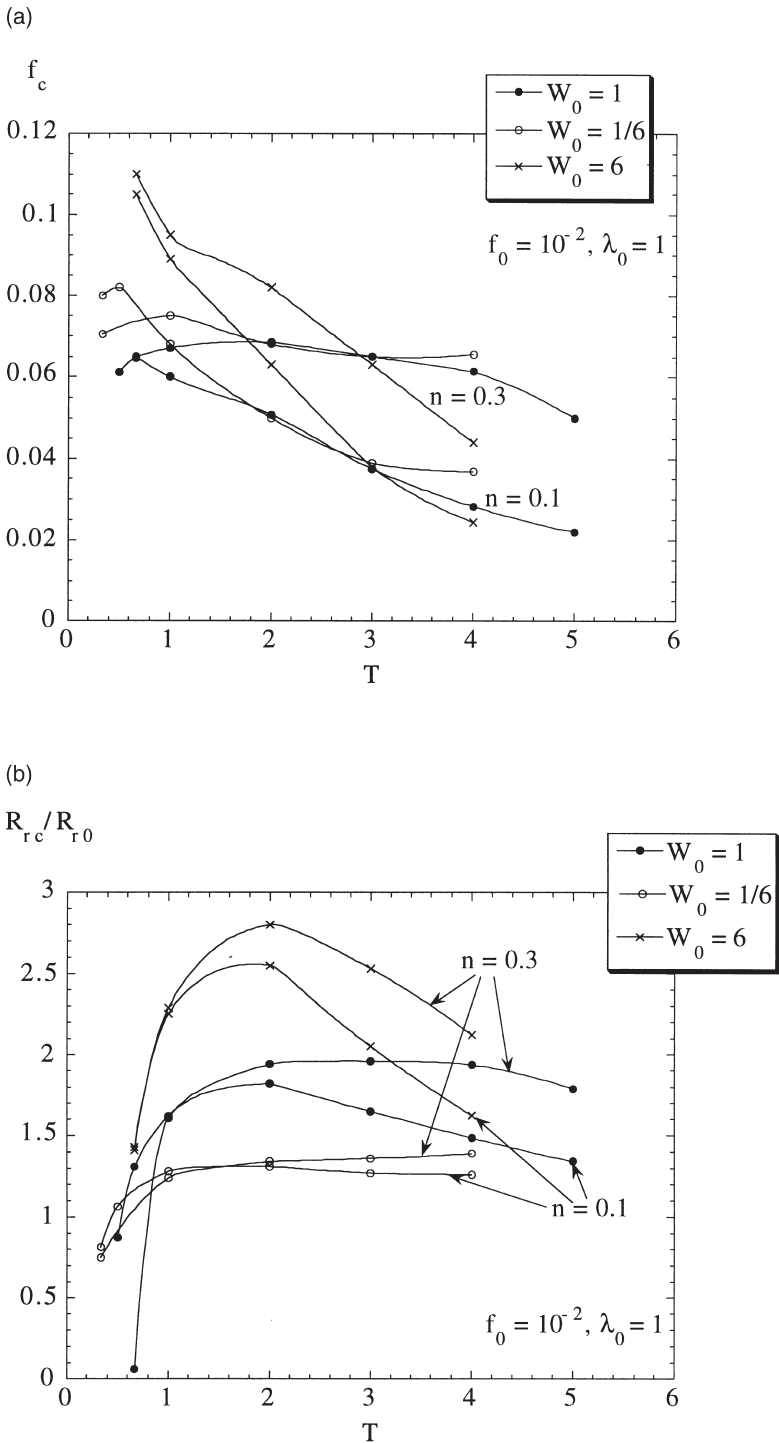


Fig. 10. Role of strain hardening on critical damage parameters at the onset of coalescence, for different initial porosity and void shapes,  $\lambda_0=1$ ; (a) critical porosity; (b) critical void radius (in the radial direction).

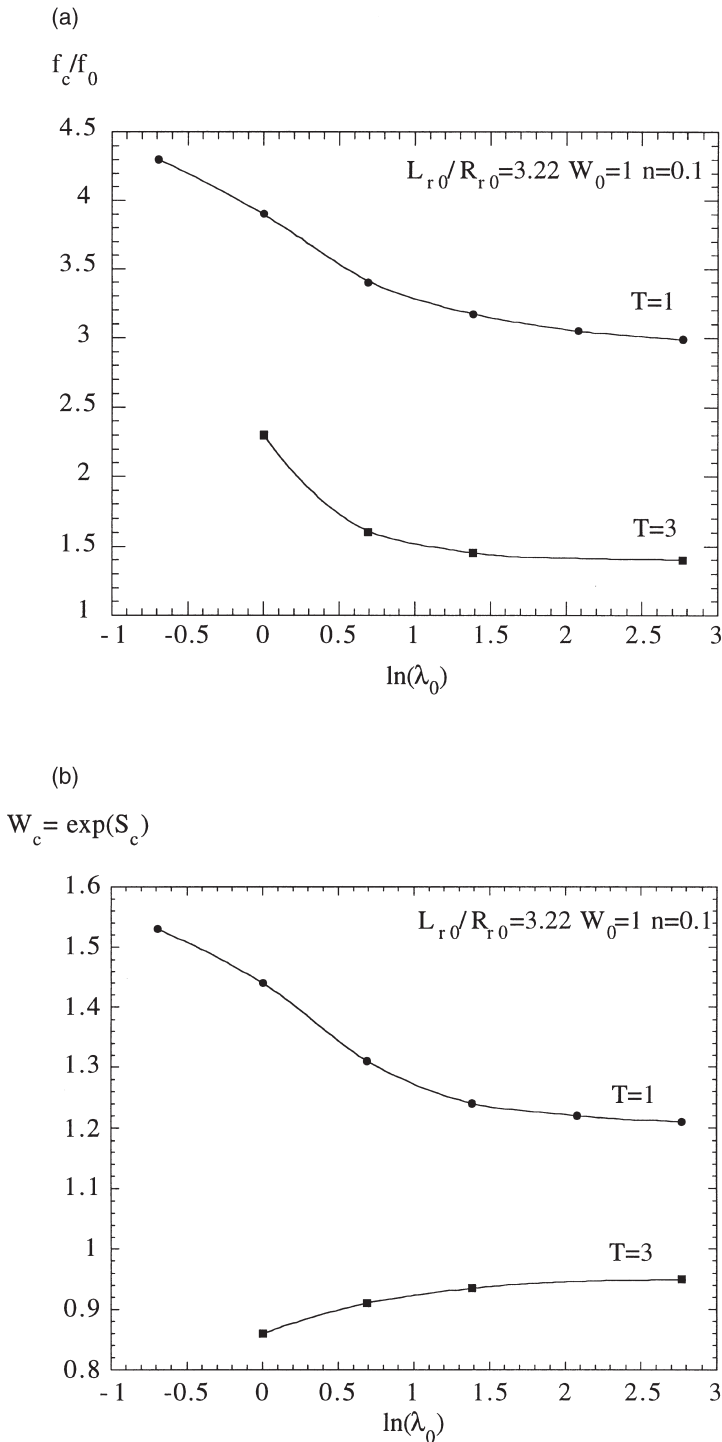


Fig. 11. Variation as a function of the elongation of the cell of (a) the critical porosity normalized by the initial porosity, and of (b) the void shape at the onset of coalescence, for cells with a constant void spacing,  $n=0.1$ ,  $W_0=1$ ,  $T=1$  and 3.

## 4. Void coalescence model

### 4.1. A criterion for the onset of void coalescence

The results presented in Section 3 have demonstrated the onset of coalescence, whether measured by  $f_c$  or  $R_{rc}$ , generally depends on  $f_0$ ,  $T$ ,  $W_0$ ,  $\lambda_0$  and  $n$ . For practical purposes, a criterion based on either  $f_c$  or  $R_{rc}$  might be attractive but, in principle, would require identification of  $f_c$  or  $R_{rc}$  as a function of  $T$  for each material. This identification process would have to be repeated each time the microstructure of a given material is modified (shape and volume fraction of inclusions, distribution, hardening of the matrix, etc.). For these reasons, a criterion based on the mechanism of plastic localization in the intervoid ligament, which was introduced in the Synopsis, is much preferred to unify the aforementioned dependencies. Details of the development of this criterion are now presented.

To motivate the model, a relatively elementary approximation is given that directly addresses the mechanism of tensile plastic localization in the intervoid ligaments. This is followed by our adoption, with minor modification, of the functional form of the void coalescence model of Thomason (1985a,b, 1990).

Diffuse plasticity throughout the cell gives way to localized deformation within the ligament with the material outside the ligament unloading elastically, as discussed in connection with Fig. 8. Consider a thin annular cylindrical disk of elastic-perfectly plastic material welded to rigid platens and constrained against flow at the outer radius, as shown in its current geometry in Fig. 12. An approximate analysis for the limit load of this configuration, with associated average true stress  $\Sigma_z$ , can be carried out along the lines of Hill's (1950) plane strain analysis of a thin plastic layer welded to and squeezed by two rigid platens. The analysis assumes the material in the disk moves outward flowing in shear and otherwise supporting only hydrostatic tension such that the three normal stresses are approximately equal. Radial equilibrium (with the approximation that the normal stresses at the void are zero) provides the applied stress as a function of the current geometry

$$\frac{\Sigma_z}{\sigma_0} = \frac{2}{3\sqrt{3}} \frac{L_r}{R_z} \left(1 - \frac{R_r}{L_r}\right)^2 \left(2 + \frac{R_r}{L_r}\right). \quad (18a)$$

The condition of zero material volume change (elastic deformations neglected) provides the relation between the current geometry and the initial geometry

$$\frac{R_z}{R_{z0}} = \frac{1 - (R_{r0}/L_r)^2}{1 - (R_r/L_r)^2}. \quad (18b)$$

The relation between  $\Sigma_z/\sigma_0$  and the overall strain  $E_z = \ln[(R_z - R_{z0})/L_{z0}]$  based on the full cell length is sketched qualitatively in Fig. 12. At low overall strain,  $\Sigma_z/\sigma_0$  from (18a) is far greater than the actual value from the cell. However, the actual solution peaks and falls (with the cell still deforming in a diffuse manner) until localization sets in, and then the actual solution merges with the artificially constrained localized

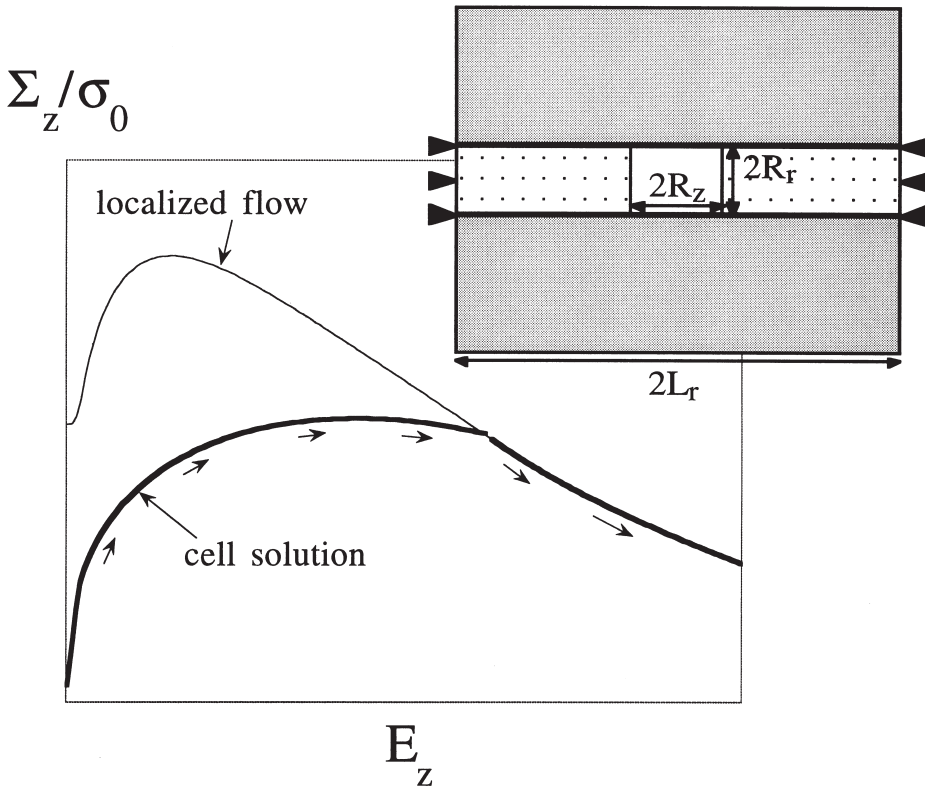


Fig. 12. Qualitative sketch of the axial stress vs axial strain curves predicted by the constrained localized solution and by the full cell solution; the transition to localization sets in when the solution for diffuse plasticity merges with the solution for a localized plastic flow.

solution. This is the transition point, and from this point on, the solution is localized within the ligament. Localization in the full cell solution is not a bifurcation phenomenon. Nevertheless, the transition to localization occurs sharply, and the competition depicted in Fig. 12 is an aid to thinking about the transition condition.

More accurate representations have been developed by Thomason (1990), who extensively studied the transition to localization for elastic-perfectly plastic solids using slip-line solutions. For axisymmetric geometries, he has proposed that the average normal stress acting on the cell at the onset of localization occurs when  $\Sigma_z$  attains  $\Sigma_z^{\text{loc}}$  where

$$\frac{\Sigma_z^{\text{loc}}}{\sigma_0} = \left[ 1 - \left( \frac{R_r}{L_r} \right)^2 \right] \left[ \alpha \left( \frac{R_z}{L_r - R_r} \right)^{-2} + \beta \left( \frac{R_r}{L_r} \right)^{-1/2} \right], \quad (19)$$

where  $\alpha=0.1$  and  $\beta=1.2$ . This condition is based solely on current geometry. By comparing this expression with our numerical results for strain hardening materials, we also find that this expression provides a reasonably accurate estimate for the

onset of localization within the cells, provided that  $\sigma_0$  is replaced by an appropriate effective flow stress for the matrix,  $\sigma_m$  (see also Zhang and Niemi, 1995), and  $\alpha$  and  $\beta$  incorporate a dependence on the strain hardening exponent  $n$ . The effective matrix stress,  $\sigma_m$ , is defined using (4) where  $\epsilon_m^p$  and  $\sigma_m$  are related through the stress–strain curve given by (17b).

Thus, with attention confined to cases where  $\Sigma_z$  is the maximum principal stress, localization is assumed to set in when  $\Sigma_z = \Sigma_z^{loc}$  where

$$\frac{\Sigma_z^{loc}}{\sigma_m} = \left[ 1 - \left( \frac{R_r}{L_r} \right)^2 \right] \left[ \alpha(n) \left( \frac{R_z}{L_r - R_r} \right)^{-2} + \beta(n) \left( \frac{R_r}{L_r} \right)^{-1/2} \right]. \tag{20}$$

The dependence on  $\alpha$  and  $\beta$  on  $n$  was determined by a fitting procedure for these coefficients to a large number of our numerical results for localization in the cell at two  $n$  values (0.1 and 0.3). The dependence on  $n$  is plotted in Fig. 13, with Thomason’s values for  $n=0$ . The coefficient  $\beta$  is almost constant and can be taken as 1.24 while

$$\alpha(n) = 0.1 + 0.217n + 4.83n^2 \quad (0 \leq n \leq 0.3), \tag{21}$$

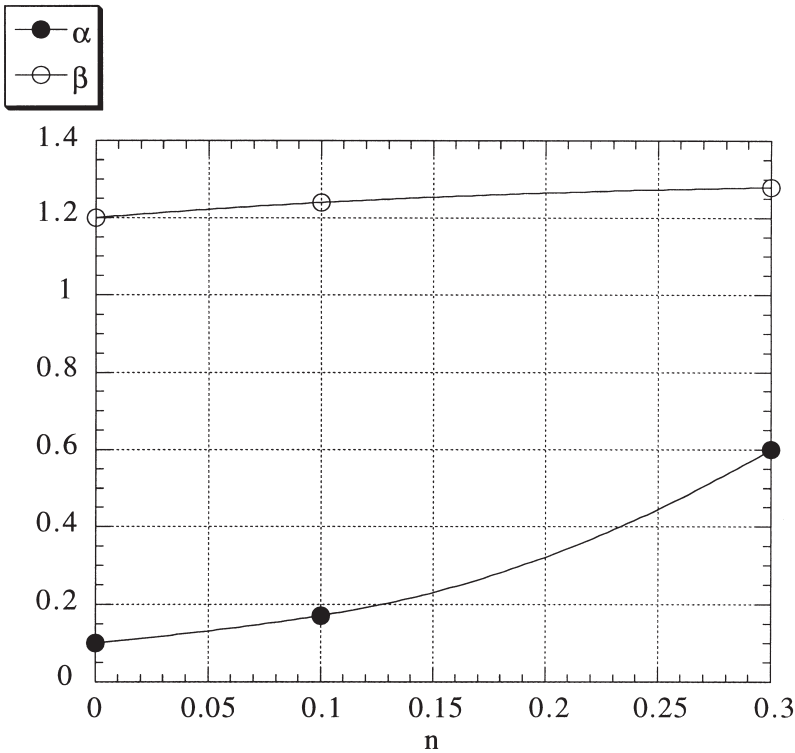


Fig. 13. Variation of the parameters of the coalescence model,  $\alpha$  and  $\beta$ , as a function of the strain hardening exponent.

which is plotted as the curve in Fig. 13. An extensive set of comparisons useful in assessing the accuracy of the criterion is presented in Fig. 14(a) for  $n=0.1$  and a wide range of triaxialities, initial volume fractions and void shapes. Each point has the coordinates

$$X = \frac{\Sigma_z^{\text{loc}}}{\sigma_m} \left[ 1 - \left( \frac{R_r}{L_r} \right)^2 \right]^{-1}, \quad Y = \left[ \alpha(n) \left( \frac{R_z}{L_r - R_r} \right)^{-2} + \beta(n) \left( \frac{R_r}{L_r} \right)^{-1/2} \right], \quad (22)$$

where  $X$  and  $Y$  are the values computed from the cell model at localization. If (20) were an exact criterion, all points would lie on the line  $X=Y$ . The extent to which they fall off the line is an indicator of the error. (The adjustment of  $\alpha$  and  $\beta$  mentioned earlier consisted of minimizing, using the least square method, the distance to the line  $X=Y$ , for all the results of Fig. 14(a) taken together.) Selected results presented in the same manner are given in Fig. 14(b) for cells with various aspect ratios, in this case all with  $T=1$ . Comparisons for the other  $n$  value is similar. An even better test of the criterion is how accurately it predicts the strain at localization, and selected comparisons will be given later in the paper.

#### 4.2. A model for the post-localization regime

Attention continues to be restricted to localizations that form perpendicular to the  $z$ -direction. Relation (20) still pertains after the onset of coalescence and  $\Sigma_z^{\text{loc}}$  is replaced by  $\Sigma_z$ , assuming the voids do not depart significantly from a spheroidal shape. If one makes this replacement and rewrites (20) using the model variables  $S$ ,  $f$ , and  $A$  in place of  $L_r$ ,  $R_r$  and  $R_z$ , one has

$$\frac{\Sigma_z}{\sigma_m} = \left[ 1 - \left( \frac{2 \exp(S-A)}{3f} \right)^{-2/3} \right] \times \left[ \alpha(n) \left( \exp(-2S) \left( \left( \frac{2 \exp(S-A)}{3f} \right)^{1/3} - 1 \right) \right)^2 + \beta(n) \left( \frac{2 \exp(S-A)}{3f} \right)^{1/6} \right]. \quad (23)$$

(This form can also be used for the localization criterion with  $\Sigma_z \equiv \Sigma_z^{\text{loc}}$ .) The additional equations for the evolution of the state variables during the post-localization stage are obtained under the approximation that elasticity, as well as any reversed plasticity, is neglected. The strains satisfy

$$\dot{E}_r = \dot{E}_r^p = \dot{E}_r^c = 0, \quad \dot{E}_z^p = \dot{E}_z. \quad (24)$$

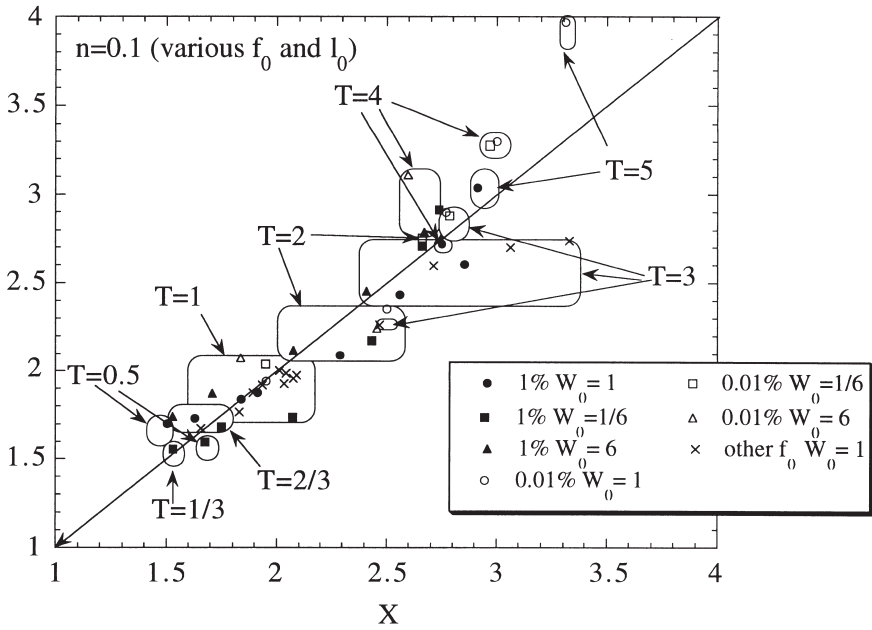
The half-height of the localization zone is approximated as  $R_z$  (i.e.  $h=R_z$ , see Fig. 1). This approximation avoids the explicit introduction of a new variable characterizing the localization band height, and it is consistent with the use of (20) or (23) regarding the void shape evolution. It also follows that  $\dot{R}_z = \dot{L}_z$ . Plastic incompressibility gives

$$\dot{f} = (1-f)\dot{E}_z, \quad (25)$$

and the evolution of  $A = \ln(L_z/L_r)$  is also elementary:  $\dot{A} = \dot{E}_z$ . The evolution of  $S$  can

(a)

Y ( $\alpha=0.17$   $\beta=1.24$ )



(b)

Y ( $\alpha=0.17$   $\beta=1.24$ )

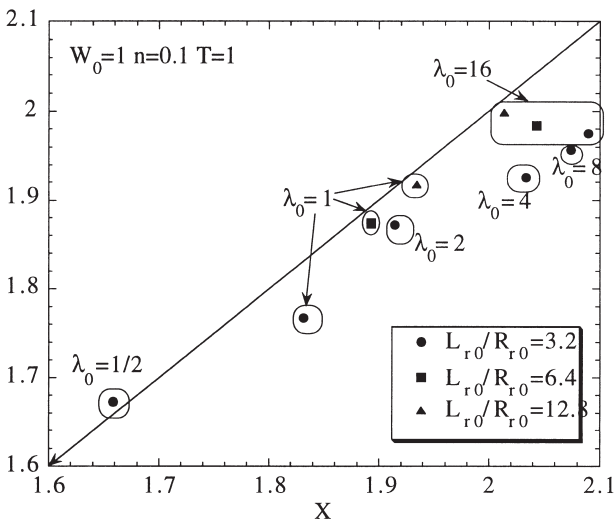


Fig. 14. Variations of  $Y$  as a function of  $X$ , as defined by Eq. (22), for void cells with  $n=0.1$ .  $\alpha$  and  $\beta$  have been chosen as to minimize the distance to the line  $X=Y$  for the entire set of void cell computations. (a) All void cell simulations performed with  $n=0.1$ . (b) A zoom in of (a) showing the effect of  $\lambda_0$  for cells with  $T=1$ . Larger  $X$  (or  $Y$ ) means a larger constraint in the intervoid ligament.

now be determined by differentiating  $\ln(R_z/R_r)$ . Then, with the aid of  $\dot{R}_z = \dot{L}_z$ , (25), and assuming volume incompressibility, one can obtain

$$\dot{S} = \frac{3}{2} \left( \left( \frac{2 \exp(2(A-S))}{3f} \right)^{1/3} - \frac{1}{3f} \right) \dot{E}_z \quad (26)$$

In order to evaluate the average yield stress  $\sigma_m$  for the matrix material in the localized band, the average effective strain rate  $\dot{\epsilon}_e^{\text{loc}}$  is needed. This is obtained from the evolution of the localized band height as

$$\dot{\epsilon}_e^{\text{loc}} = \frac{\dot{h}}{h} = \frac{\dot{R}_z}{R_z} = \left( \frac{2 \exp(2(A-S))}{3f} \right)^{1/3} \dot{E}_z. \quad (27)$$

At the onset of localization,  $\dot{\epsilon}_e^{\text{loc}} = \dot{\epsilon}_m^p$ , which is known. In the post localization response,  $\sigma_m$  is derived from  $\epsilon_e$  using the uniaxial flow curve (17b).

## 5. Analysis of the full model for void growth and coalescence

### 5.1. The extended Gurson model for spheroidal void growth

In this section, the model will be completed by specification of the yield function and flow potential for materials with aligned spheroidal voids. Comparisons are then made between predictions from the model and those from full cell model computations. One conclusion uncovered in the analysis of void coalescence is that the void aspect ratio significantly affects void coalescence, even when the void is initially spherical. In other words, the void coalescence model cannot simply be coupled to a damage model based on spherical void growth. The full model must account for void shape evolution.

Constitutive models incorporating void shape effect have been recently proposed in the literature (Gologanu et al. 1993, 1994; Ponte Castañeda and Zaidman, 1994). Gologanu et al. (1995) extended the Gurson model, employing a rigorous micromechanical analysis, considering both prolate and oblate spheroidal voids. The extension retains a form similar to that of the Gurson model while introducing plastic anisotropy resulting from the non-spherical void evolution. For such a purpose, the void aspect ratio,  $S$ , comes into play, for which an evolution law is also derived. The main equations of the extended model for the axisymmetric case are

$$\Phi = \frac{C}{\sigma_m^2} (\Sigma_z - \Sigma_r + \eta \Sigma_h)^2 + 2q(g+1)(g+f) \cosh\left(\kappa \frac{\Sigma_h}{\sigma_m}\right) - (g+1)^2 - q^2(g+f)^2, \quad (28)$$

$$\dot{f} = (1-f) \dot{E}_{kk}^p, \quad (29)$$

$$\dot{S} = (1 + h_s h_r h_f) (\dot{E}_z^p - \dot{E}_r^p) + h_{sr} \dot{E}_{kk}^p, \quad (30)$$

$$\sigma_m \dot{\epsilon}_m^p (1-f) = \Sigma_{ij} \dot{E}_{ij}^p, \quad (31)$$

$$\dot{E}_{ij}^p = \gamma \frac{d\Phi}{d\Sigma_{ij}}, \quad (32)$$

with

$$\Sigma_h = 2\alpha_2 \Sigma_r + (1 - 2\alpha_2) \Sigma_z. \quad (33)$$

A description of the terms in these equations follows. The heuristic parameter of Tvergaard,  $q$ , depends on  $n$ ,  $S$ ,  $T$ , and  $f_0$ , as specified in Appendix A (see also Koplik and Needleman, 1988; Perrin and Leblond, 1990; Gologanu, 1997). The phenomenological energy balance (31) for plastic work originally proposed by Gurson (1977) is retained in our version. (This equation is not used in the Gologanu et al. model which assumes perfect plasticity. A more rigorous approach for incorporating hardening has been proposed by Leblond et al. (1995) for the case of spherical void growth). The parameter  $g$  can be interpreted as “the fictitious porosity obtained by replacing the real spheroidal void by a spherical one with radius equal to the focal distance” (Gologanu et al., 1995). It is set to zero for prolate or spherical voids. The quantities  $C$ ,  $\eta$ ,  $\alpha_2$ ,  $\kappa$ ,  $g$ , and  $h_{sf}$  are functions of  $S$  and  $f$ ;  $h_s$  is a function of  $S$ ;  $h_f$  is a function of  $f$ ;  $h_T$  is a function of the stress triaxiality  $T$  and  $n$ . The functional dependencies of these quantities are specified in Appendix A. The Gurson model is recovered when  $S=0$ . The rate of  $S$  depends on both the deviatoric and hydrostatic parts of the strain rate tensor. In addition to the  $q$  factor retained here, the determination of some parameters of Eq. (30) is the only part of the model which does not fully emerge from the micromechanical analysis. It has been calibrated with the aid of numerical results. One possible extension of this model to arbitrary multiaxial stress states can be found in Gologanu et al. (1995). We emphasize again that the Gurson model and its extension introduced here are intended exclusively as a constitutive relation to be used in numerical (usually finite element) calculations. The additional quantities introduced above in the extended model do not significantly increase the computational complexity of the model.

As in the conventional Gurson model, the relation giving the plastic strain rates as a function of the stress rates is obtained using the consistency condition for plastic loading

$$\dot{\Phi} = 0 \quad (34)$$

Isotropic elasticity is assumed. The model is supplemented by the void coalescence model described in Section 4, relations (23) to (27). In the present work, the model is integrated numerically using an explicit forward Euler scheme. At each increment of the calculation the right- and left-hand sides of Eq. (23) are evaluated using the current values of  $S$ ,  $f$ , and  $A$ , while  $L_r$  and  $L_z$ , required to compute  $A$ , are given by

$$\frac{\dot{L}_z}{L_z} = \dot{E}_z \quad \text{and} \quad \frac{\dot{L}_r}{L_r} = \dot{E}_r \quad (35)$$

## 5.2. Assessment of the full model

Comparisons are now made between the predictions obtained with the full extended model for void growth and coalescence and void cell simulations. These

results will provide additional assessment of the void coalescence model. Fig. 15(a–f) present results for  $f_0=10^{-4}$  at triaxialities  $T=1$  (a–c) and  $T=3$  (d–f) for initial void shapes  $W_0=1/6, 1$  and  $6$ . For each stress triaxiality, the evolution of the effective stress,  $\Sigma_e$ , the porosity,  $f$ , and the void shape parameter,  $S$ , are given as a function of the effective strain  $E_e$ . A cross on the void cell results indicates the onset of void coalescence, while a circle indicates the onset of void coalescence predicted by applying Eq. (20) or Eq. (23) with all the parameters taken from the void cell computations. (When the model tends to predict a larger coalescence strain than given by the void cells, the parameters used in (20) coming from the void cells were extrapolated from their values before the onset of coalescence as if the localization did not happen in the void cells, i.e. as if diffuse plasticity carries on in the cell.) The difference in strain between the circle and the cross indicates the error resulting only from the application of the criterion for the onset of coalescence. It is evident that the criterion for the onset of coalescence is highly accurate regardless of the void shape (Fig. 15(a, d)). In fact, when Eq. (20) is used together with the enhanced Gurson model, the error on the prediction of the onset of coalescence mainly results from the error in computing the porosity and the other parameters with the constitutive model.

At  $T=1/3$  (results not shown), no coalescence is observed at any of the initial void shapes, and the porosity remains very small such that all the stress–strain curves essentially coincide with the curve for  $f_0=0$ . At  $T=1$  and  $3$ , the ductility predicted by the full model overestimates the value given by the void cells (Fig. 15(a, d)). This is due to an underestimation of the void growth rate by the model before coalescence (see Fig. 15(b, e)). The acceleration of void growth which starts around the peak stress (before localized yielding sets in) is not captured by the extended model even though the  $q$  factor is used. This effect can also be detected in results by Koplik and Needleman (1988). Void shape evolution is correctly modeled during the growth phase (Fig. 15(c, f)). After the onset of coalescence, the fidelity of the model results for shape evolution deteriorates at low triaxiality (see Fig. 15(c) for  $T=1$ ), because the localization band is smaller than  $R_z$  used in the post-coalescence derivation in Section 4. Nevertheless, the stress–strain predictions in the post-localization regime are quite good, and such predictions are one of the main objectives of the model. The slope of the stress–strain curve could be reasonably approximated as being constant after localization to make easier the implementation in a finite element code (see also Ruggieri et al., 1996; Xia and Shih, 1995a; Gao et al., 1998).

Fig. 16(a–c) presents results for a significantly larger initial void volume fraction:  $f_0=10^{-2}$ . The results are now given only in terms of the stress–strain curves in the axial direction for three triaxialities and three initial void shapes. Fig. 16(a) for  $T=1/3$  shows that the full model correctly predicts coalescence for the very oblate void, and no coalescence for  $W_0=1$  and  $W_0=6$ . (Both the model and the void cell calculations predict a saturation of porosity with increasing strain.) This is a remarkable result which would never be obtained from models not incorporating void shape effects. However, it is important to mention that in cases of small triaxiality, the predictions of the model are sensitive to small variations in  $L_{r0}/R_{r0}$ . The full model is not robust at very small stress triaxiality and can only be considered as giving qualitative predictions, although the coalescence model alone is again very accurate.

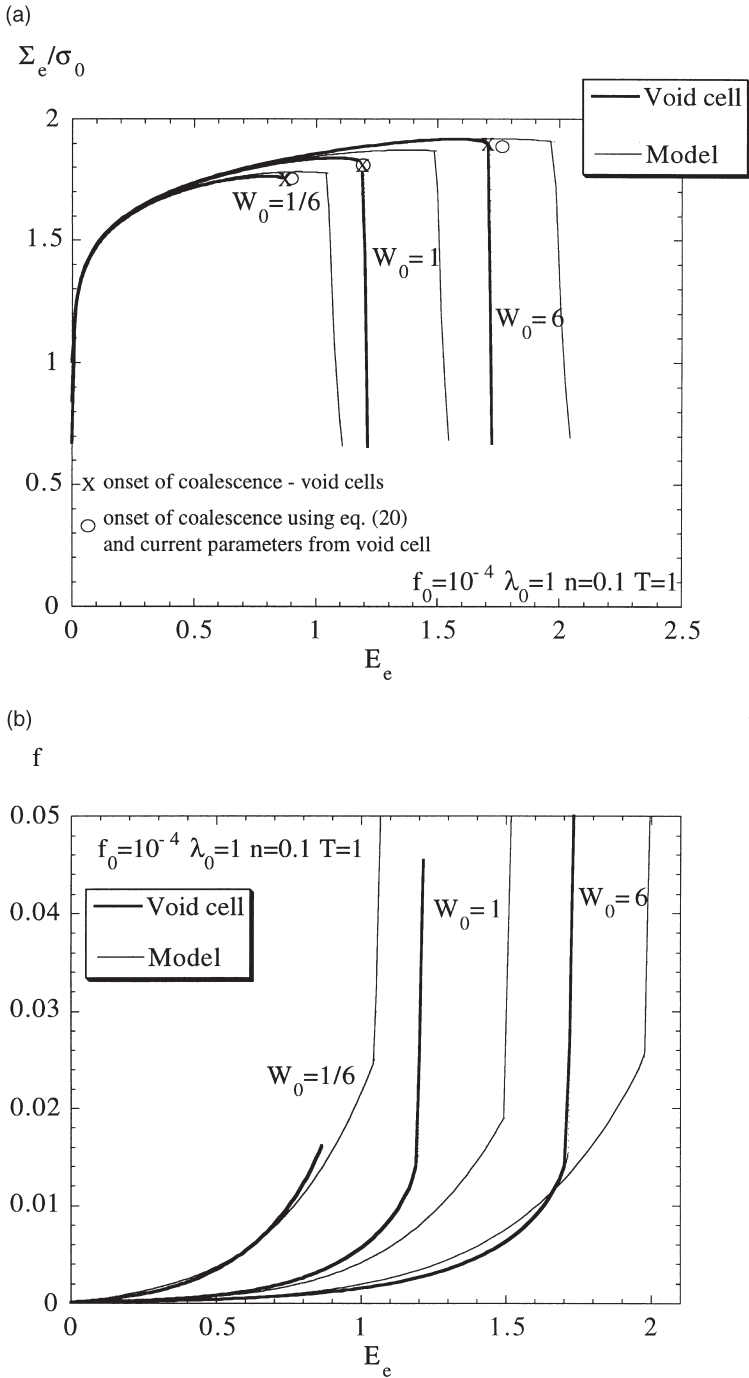
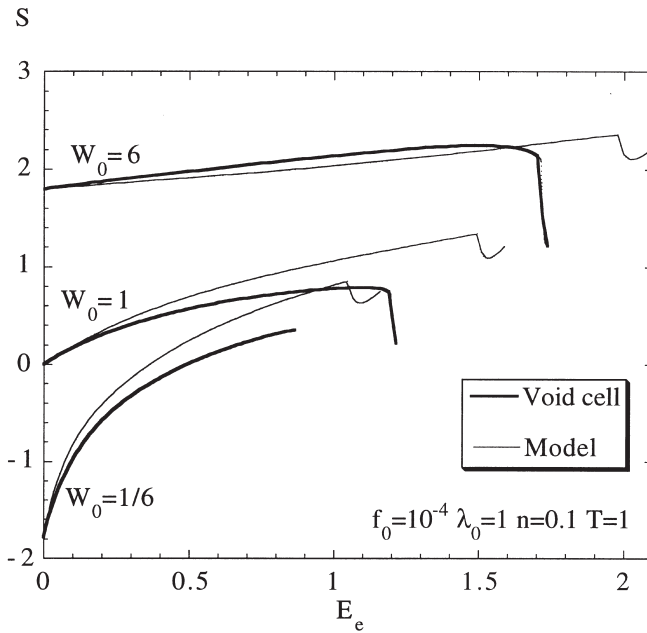


Fig. 15. Comparison between void cell computations and the model for  $n=0.1$ ,  $f_0=10^{-4}$ ,  $\lambda_0=1$  and  $W_0=1/6$ , 1 and 6; (a) effective stress vs effective strain curves,  $T=1$ ; (b) porosity variation,  $T=1$ ; (c) void shape variation,  $T=1$ ; (d) effective stress vs effective strain curves,  $T=3$ ; (e) porosity variation,  $T=3$ ; (f) void shape variation,  $T=3$ .

(c)



(d)

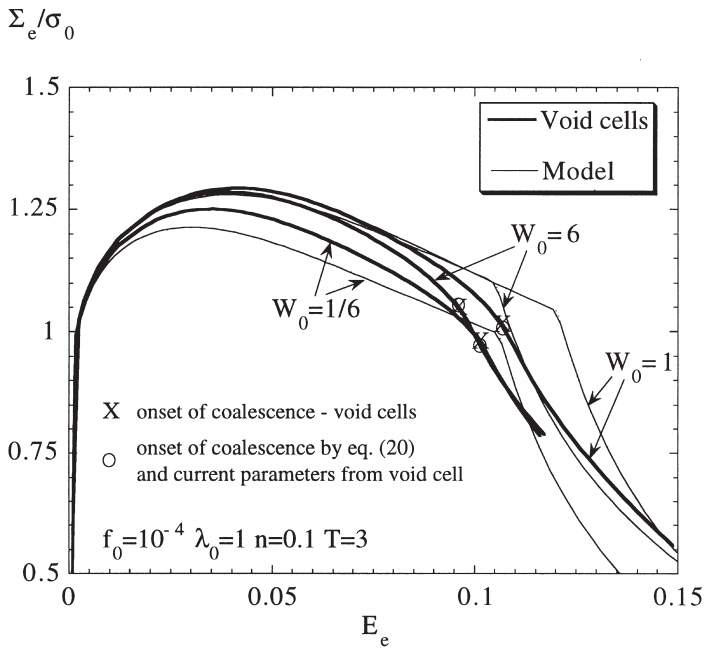


Fig. 15. (continued)

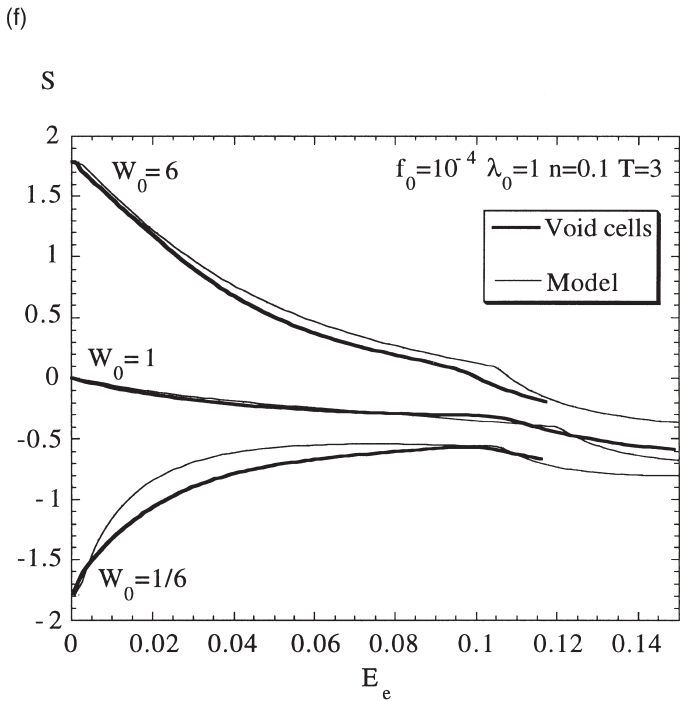
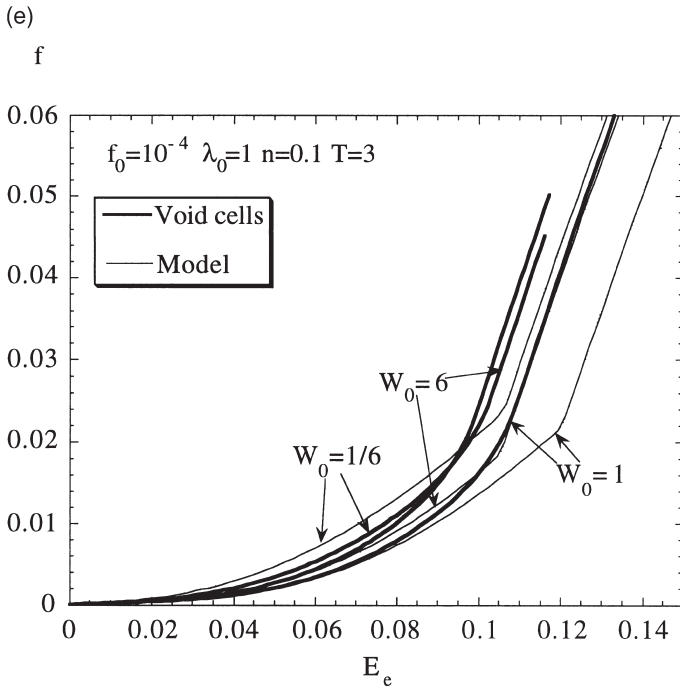


Fig. 15. (continued)

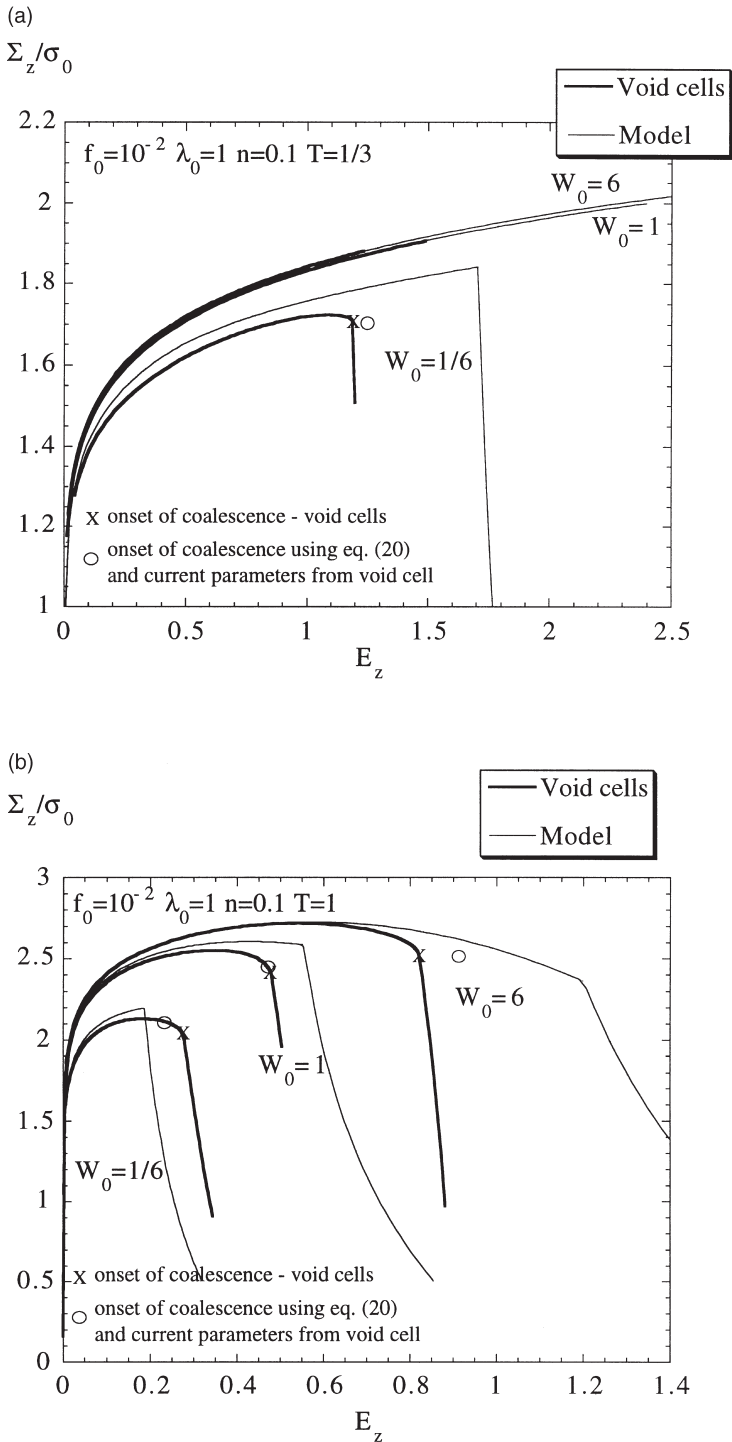


Fig. 16. Comparison between the axial stress–strain curves predicted by the void cell computations and the model for  $n=0.1$ ,  $f_0=10^{-2}$ ,  $\lambda_0=1$  and  $W_0=1/6, 1$  and  $6$ ; (a)  $T=1/3$ ; (b)  $T=1$ ; (c)  $T=3$ .

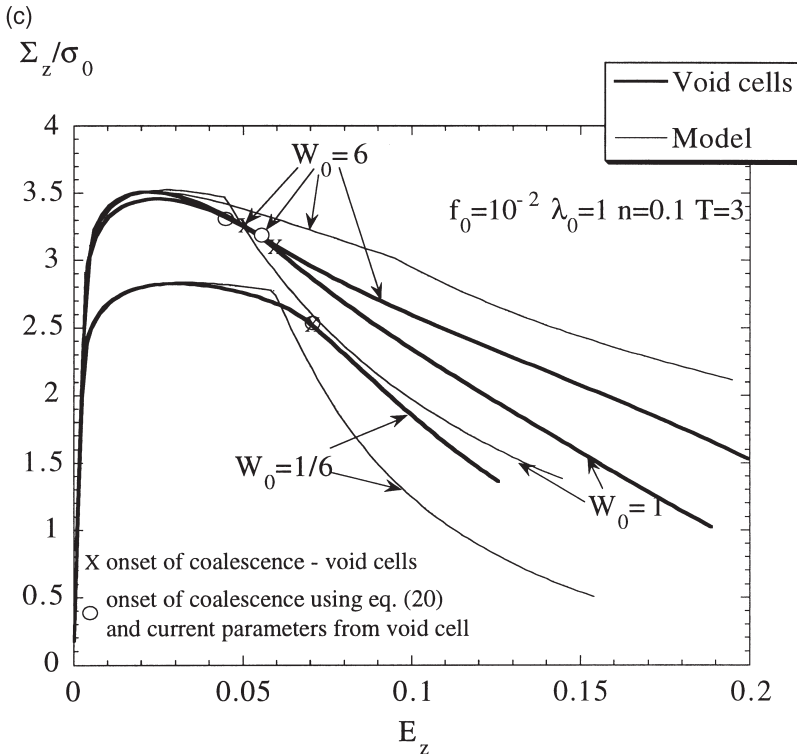


Fig. 16. (continued)

At both  $T=1$  and  $3$ , the ductility for the oblate voids is underestimated by the extended model ( $W_0=1/6$ ). This underestimation results from an overestimation of the void growth rate for oblate voids when the initial porosity becomes important ( $>10^{-2}$ ). For all the other cases, underestimation of the void growth rate by the model before coalescence is observed. At both  $T=1$  and  $3$ , the onset of coalescence is adequately modeled by Eq. (20) except for  $W_0=1$  and  $T=3$ , where a 20% error is observed. At  $T=1$ , for a highly prolate initial void,  $W_0=6$ , the post-localization stress–strain curve predicted by the model is less steep than the cell model result, again because of the approximation used for the height of the localization zone. At  $T=3$ , the post-localization model gives excellent results.

Fig. 17 shows one set of results for a high strain hardening material:  $n=0.3$  (at  $T=1$ ). Note that the error coming from the void coalescence model alone is evident for the oblate void. Use of (31) at high strain hardening incurs error (Leblond et al., 1995). Results of a similar quality have been observed at other stress triaxialities ( $T=2/3, 2$  and  $4$ ) for  $f_0=10^{-2}$  or  $10^{-4}$  and  $n=0.1$  or  $0.3$ .

Fig. 18(a, b) address the ability of the model to account for the effect of the void cell aspect ratio  $\lambda_0$ . The agreement between the extended model and the cell model calculations is generally quite good both before and after localization, especially at

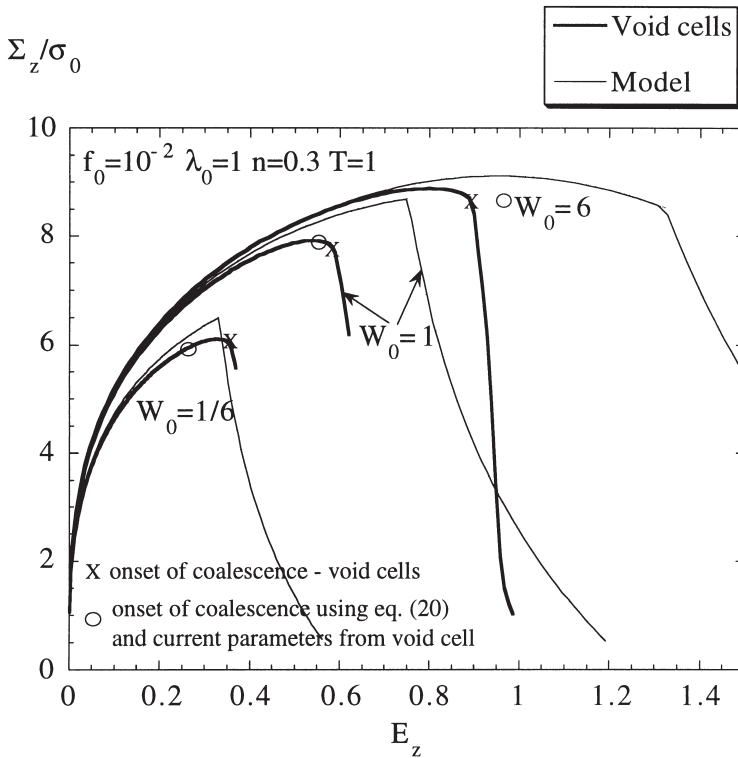


Fig. 17. Comparison between the axial stress–strain curves predicted by the void cell computations and the model for  $n=0.3$ ,  $f_0=10^{-2}$ ,  $\lambda_0=1$  and  $W_0=1/6$ , 1 and 6, at  $T=1$ .

large stress triaxiality. The increasing rate of unloading for larger  $\lambda_0$  is captured quite perfectly.

## 6. Conclusion and perspectives

To conclude, some remarks comparing the present extension with the versions of the Gurson model currently in use will be reiterated (see Table 1). The new model only depends on the initial values of the state variable and thus avoids the use of critical porosities (for the onset of coalescence and for final separation). Three major advantages accrue: (i) the approach is more fundamental; (ii) prior research, including the present, has shown that critical porosities are not material properties but depend on the stress state; (iii) critical porosities are not easily determined experimentally. The two additional microstructural characteristics of the new model,  $S_0$  and  $\lambda_0$ , can be obtained from the same metallographic analysis performed to ascertain  $f_0$  and  $L_0$ . The only parameter which has to be tuned in order to reproduce the void cell simulations is the parameter  $q$  (but this tuning has been done once for all, see

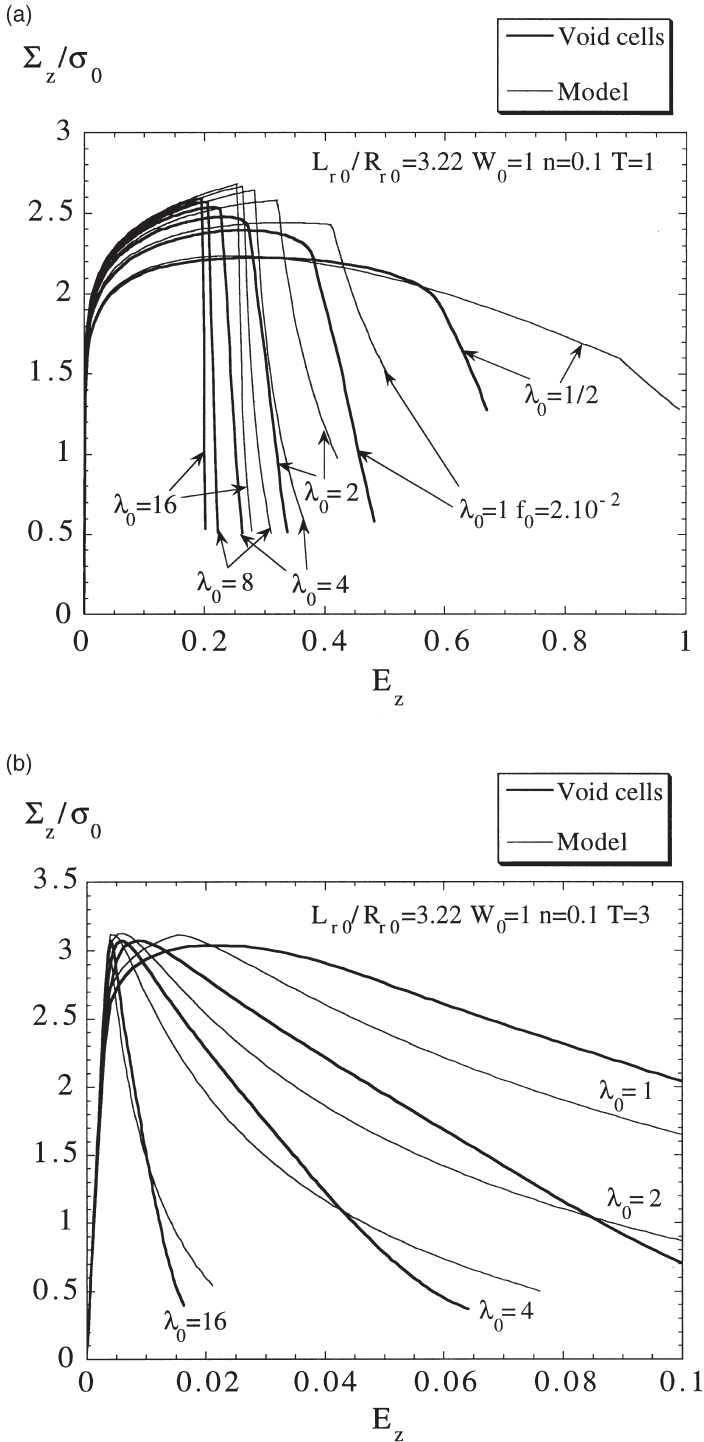


Fig. 18. Comparison between the axial stress–strain curves predicted by the void cells and the model for various cell aspect ratios at constant void spacing,  $W_0=1$ ,  $n=0.1$ ; (a)  $T=1$ ; (b)  $T=3$ .

Appendix A). The incorporation of the void shape avoids the use of the second tuning factor  $q_2$  introduced by Tvergaard (1981, 1990). Although the new version of the model is somewhat more complex than earlier versions, it does not make use of more parameters. It enables new issues to be addressed involving the role of relative void spacing and void shape.

The comparison with the void cell simulations has established that the full void growth/coalescence model is able to account for variations in all the characteristic parameters of the representative volume element of Fig. 1: porosity, void shape, cell aspect ratio, stress triaxiality, for a wide range of matrix flow behavior. The criterion for the onset of coalescence has been shown to be very accurate for most of the cases analyzed in this work. Most importantly, behavior at low and large stress triaxiality are adequately encompassed by the same model.

### 6.1. Limitations and possible improvements

- *Void nucleation.* The present work does not discuss void nucleation which plays an important role in the void process in some materials (e.g. Pineau, 1992). Void nucleation models could easily be fitted within the present framework.
- *Void growth model.* Even with the  $q$  factor, it has been proved that an acceleration of the void growth rate before the onset of coalescence is not accounted for correctly. Indeed, the  $q$  factor has been fitted for the initial void growth rate and not to give the right porosity around void coalescence, which would be a markedly more ad hoc procedure. The use of the heuristic  $q$  factor (or  $q_1$  and  $q_2$  in the version of the model by Tvergaard, 1981) is a remnant weakness of the Gurson model. The void growth prediction could be improved by considering the RVE as a combination of a porous and a non-porous zone (Gologanu, 1997). The height of the porous zone is defined such that the confocality assumption used to derive the model is respected (see Appendix A). The incorporation of more adequate hardening behavior into the model offers additional room for improvement (see Leblond et al., 1995; Pardoen and Delannay, 1998a,b). Finally, at very low stress triaxiality (typically  $T < 0.5$ ), the presence of the inclusion which prevents the radial contraction of the void has to be accounted for (Fleck et al., 1989; Steglich and Brocks, 1997; Pardoen and Delannay, 1998a; Siruguet, 2000).
- *Onset of void coalescence.* For high strain hardening, the significant variation in  $\alpha$  with the strain hardening exponent  $n$  is a problem when dealing with materials presenting different hardening stages. A sounder micromechanical model for coalescence which incorporates strain hardening would be a welcomed extension of the present work. A complete coalescence model would also incorporate the possibility of a microscopic shear localization at an angle like those observed in plane strain (e.g. Faleskog and Shih, 1997) or 3D computations (Richelsen and Tvergaard, 1994; Kuna and Sun, 1996). Inhomogeneity in the distribution of cavities has been shown not to significantly affect void growth (Needleman and Kushner, 1990). However, a huge effect on coalescence is obviously expected as void spacing is the most influent parameter. For the time being, material heterogeneity can be accounted for in our model, by adjusting  $L_{r0}/R_{r0}$  to the mean dis-

tance between closest cavities (Pardoen et al., 1998) and not to the average distance between neighboring cavities.

- *Void coalescence.* Accounting for the presence of a second population of voids in the ligament during the coalescence phase would be necessary to adequately represent the behavior of many metal alloys (Faleskog and Shih, 1997). The approximation of a constant height of the microscopic localization band inside the ligament also requires more detailed analysis.

## 7. Addendum

During the process of publication, the authors have discovered additional work by Gologanu (1997), in which he proposes a model (growth and coalescence) which has many resemblances with the model addressed in this paper.

## Acknowledgements

T.P. acknowledges a fellowship from the Fonds National de la Recherche Scientifique (F.N.R.S.) Belgium, and postdoctoral fellowships from the Belgian American Educational Foundation Inc. (B.A.E.F.) and the Université catholique de Louvain (U.C.L.). The work of JWH was supported in part by the NSF grant CMS-9634632 and in part by the Division of Engineering and Applied Sciences, Harvard University. The authors thank the anonymous reviewer and Dr A. Benzerga, Dr P. Onck, and Dr C. Landis for valuable comments.

## Appendix A. The void growth model

The enhanced Gurson model proposed by Gologanu et al. (1995) is based on the analysis of the growth of a spheroidal void in a finite, perfectly plastic solid with an outer confocal surface subjected to homogeneous straining. For mathematical convenience, the model is not expressed in terms of  $f$  and  $S$ , but mainly in terms of the inner and outer eccentricity,  $e_1$  and  $e_2$ , which are uniquely related to  $f$  and  $S$  by the following equations,

$$e_1 = \sqrt{1 - \frac{1}{\exp(2|S|)}}, \quad (\text{A1})$$

$$\frac{(1-e_2^2)}{e_2^3} = \frac{1(1-e_1^2)}{f e_1^3} \quad \text{“prolate shape, } p: S \geq 0\text{”}, \quad (\text{A2a})$$

$$\frac{\sqrt{(1-e_2^2)}}{e_2^3} = \frac{1\sqrt{(1-e_1^2)}}{f e_1^3} \quad \text{“oblate shape, } o: S < 0\text{”}. \quad (\text{A2b})$$

The parameters used in the models (28)–(33) are expressed in terms  $e_1$  and  $e_2$ :

$$g=0 \text{ “p”}, \tag{A3a}$$

$$g=\frac{e_2^3}{\sqrt{1-e_2^2}} \text{ “o”}, \tag{A3b}$$

$$\alpha_2=\frac{(1+e_2^2)}{(3+e_2^4)} \text{ “p”}, \tag{A4a}$$

$$\alpha_2=\frac{(1-e_2^2)(1-2e_2^2)}{(3-6e_2^2+4e_2^4)} \text{ “o”}, \tag{A4b}$$

$$\kappa^{-1}=\frac{1}{\sqrt{3}}+\frac{1}{\ln f}\left(\left(\sqrt{3}-2\right)\ln\left(\frac{e_1}{e_2}\right)\right)+\frac{1}{\ln f}\left(\frac{1}{\sqrt{3}}\ln\left(\frac{3+e_2^2+2\sqrt{3+e_2^4}}{3+e_1^2+2\sqrt{3+e_1^4}}\right)\right) \tag{A5a}$$

$$+\ln\left(\frac{\sqrt{3+\sqrt{3+e_1^4}}}{\sqrt{3+\sqrt{3+e_2^4}}}\right) \text{ “p”},$$

$$\kappa^{-1}=\frac{2}{3}+\frac{2/3(g_f-g_1)+2/5(g_f^{5/2}-g_1^{5/2})(4/3-g_f^{5/2}-g_1^{5/2})}{\ln(g_f/g_1)} \text{ “o”}, \tag{A5b}$$

with

$$g_f=\frac{g}{g+f} \text{ and } g_1=\frac{g}{g+1} \text{ “o”}, \tag{A6}$$

$$\eta=\frac{\kappa q(1-f)(g+1)(g+f)sh}{(g+1)^2+q^2(g+f)^2+2q(g+1)(g+f)[\kappa(\alpha_1-\alpha_2)sh-ch]}, \tag{A7}$$

with

$$sh\equiv\sinh(2\kappa(\alpha_1-\alpha_2)) \text{ and } ch\equiv\cosh(2\kappa(\alpha_1-\alpha_2)), \tag{A8}$$

$$\alpha_1=\frac{[e_1-(1-e_1^2)\tanh^{-1}(e_1)]}{2e_1^3} \text{ “p”}, \tag{A9a}$$

$$\alpha_1=\frac{[-e_1(1-e_1^2)+\sqrt{1-e_1^2}\sin^{-1}(e_1)]}{2e_1^3} \text{ “o”}, \tag{A9b}$$

$$C=-\frac{\kappa q(g+1)(g+f)sh}{\eta[1-f+2\eta(\alpha_1-\alpha_2)]}, \tag{A10}$$

$$h_s = \frac{9\alpha_1 - \alpha_1^G}{21 - 3\alpha_1}, \tag{A11}$$

with

$$\alpha_1^G = \frac{1}{(3 - e_1^2)} \text{ “p”}, \tag{A12a}$$

$$\alpha_1^G = \frac{(1 - e_1^2)}{(3 - 2e_1^2)} \text{ “o”}, \tag{A12b}$$

$$h_f = (1 - \sqrt{f})^2, \tag{A13}$$

$$h_{sf} = \left( \frac{1 - 3\alpha_1}{f} + 3\alpha_2 - 1 \right). \tag{A14}$$

The heuristic factor  $q$  in (28) reflects limitations of the model to properly account for interaction between cavities. The following expression for  $q$  is used:

$$q = \tan^{-1}(4(2.5 - T)) \left| \frac{b(S, f, n) - 1}{\pi} \right| + \frac{b(S, f, n)}{2} + \frac{1}{2}, \tag{A15}$$

with

$$b = 1 + (0.655 - 1.75n - 0.5334\sqrt{f}) \left( \frac{1}{2} + \frac{\tan^{-1}(2(1-2))}{\pi} - 0.0288e^{-1.08(0.2+s)} \right) \tag{A16}$$

The last expression is valid for  $S > -2$ ,  $f < 5 \times 10^{-2}$  (and thus not for penny-shape cracks). This equation is a good fit of a large number of values of  $q$  obtained by adjusting the void growth rates predicted by the model to the void growth rates predicted by void cell computations in the early stages of straining. A unique equation for  $q$  presenting continuous derivatives with respect to the state dependent variables was deemed attractive for numerical integration. The necessity of decreasing the value of  $q$  for increasing  $n$  has already been discussed by several authors (e.g. Koplik and Needleman, 1988; Sovik and Thaulow, 1997). The effect of  $f$  on  $q$  was addressed by Perrin and Leblond (1990) for the case of perfect plasticity and by Sovik and Thaulow (1997). The latter authors also analyzed the effect of  $T$  on  $q$ . Elongated prolate voids give rise to a value of  $q \approx 1$  for all values of  $n$ . This is consistent with the Gurson model for cylindrical voids, exact in that case, and which requires  $q=1$ .

Finally,  $h_T$  has been adjusted to give the best predictions for the void shape rates at the two strain hardening levels (only valid for  $T < 4$ ):

$$h_T = 1 - 0.555T^2 - 0.045T^4 + 0.002T^6, n=0.1 \tag{A17}$$

and

$$h_T = 1 - 0.54T^2 + 0.034T^4 - 0.00124T^6, \quad n = 0.3. \quad (\text{A18})$$

The function  $h_T$  for  $n=0.1$  is close to the one proposed by Gologanu et al. (1995) for perfect plasticity.

## References

- ABAQUS Version 5.7, 1997. User's Manual. Hibbit, Karlsson & Sorensen, Providence, RI.
- Achon, P., 1994. Comportement et Ténacité d'Alliages d'Aluminium à Haute Résistance. Thèse de doctorat, Ecole Nationale Supérieure des Mines de Paris.
- Ashby, M.F., Blunt, F.J., Bannister, M., 1989. Flow characteristics of highly constrained metal wires. *Acta Metallurgica* 37, 1847–1857.
- Becker, R., 1987. The effect of porosity distribution on ductile failure. *Journal of the Mechanics and Physics of Solids* 35, 577–599.
- Becker, R., Smelser, R.E., 1994. Simulation of strain localization and fracture between holes in an aluminum sheet. *Journal of the Mechanics and Physics of Solids* 42, 773–796.
- Becker, R., Smelser, R.E., Richmond, O., Appleby, E.J., 1989. The effect of void shape on void growth and ductility in axisymmetric tension tests. *Metallurgical Transactions A* 20, 853–861.
- Benzerga, A.A., Besson, J., Pineau, A., 1999. Coalescence-controlled anisotropic ductile fracture. *Journal of Engineering Materials and Technology* 121, 221–229.
- Bethmont, M., Rousselier, G., Kussmaul, K., Sauter, A., Jovanovic, A., 1990. The local approach of fracture and its application to a thermal shock experiment. *Nuclear Engineering and Design* 119, 249–261.
- Bilby, B.A., Howard, I.C., Li, Z.H., 1993. Prediction of the first spinning cylinder test using ductile damage theory. *Fatigue and Fracture of Engineering Materials and Structures* 16, 1–20.
- Bourcier, B.J., Koss, D.A., Smelser, R.E., Richmond, O., 1986. The influence of porosity on the deformation and fracture of alloys. *Acta Metallurgica* 34, 2443–2453.
- Brocks, W., Klingbeil, D., Kunecke, G., Sun, D.-Z., 1995a. Application of the Gurson model to ductile tearing resistance. In: Kirk, M., Bakker, A. (Eds.), *Constraint Effects in Fracture Theory and Applications*, Vol. 2. American Society for Testing and Materials, Philadelphia, pp. 232–252 (ASTM STP 1244).
- Brocks, W., Sun, D.Z., Höning, A., 1995b. Verification of the transferability of micromechanical parameters by cell model calculations with visco-plastic materials. *International Journal of Plasticity* 11, 971–989.
- Budiansky, B., Hutchinson, J.W., Slutsky, S., 1982. Void growth and collapse in viscous solids. In: Hopkins, H.G., Sewell, M.J. (Eds.), *Mechanics of Solids, The Rodney Hill 60th Anniversary Volume*. Pergamon Press, pp. 13–45.
- Chu, C.C., Needleman, A., 1980. Void nucleation effects in biaxially stretched sheets. *Journal of Engineering Materials and Technology* 102, 249–256.
- Cox, T.B., Low, J.R., 1974. An investigation of the plastic fracture of AISI 4340 and 18 nickel-200 grade maraging steels. *Metallurgical Transactions A* 5, 1457–1470.
- Dubensky, E.M., Koss, D.A., 1987. Void/pore distributions and ductile fracture. *Metallurgical Transactions A* 18, 1887–1895.
- d'Escatha, Y., Devaux, J.C., 1979. Numerical study of initiation, stable crack growth and maximum load with a ductile fracture criterion based on the growth of holes. In: Landes, J.D., Begley, J.A., Clarke, G.A. (Eds.), *Elastic-Plastic Fracture*. American Society for Testing and Materials, Philadelphia, pp. 229–248 (ASTM STP 668).
- Faleskog, J., Shih, C.F., 1997. Micromechanics of coalescence — I. Synergistic effects of elasticity, plastic yielding and multi-size-scale voids. *Journal of the Mechanics and Physics of Solids* 45, 21–45.
- Fleck, N.A., Hutchinson, J.W., Tvergaard, V., 1989. Softening by void nucleation and growth in tension and shear. *Journal of the Mechanics and Physics of Solids* 37, 515–540.

- Gao, X., Faleskog, J., Shih, C.F., 1998. Cell model for nonlinear fracture analysis — II. Fracture-process calibration and verification. *International Journal of Fracture* 89, 374–386.
- Gologanu, M., 1997. Etude de Quelques Problèmes de Rupture Ductile des Métaux. Thèse de Doctorat de l'Université Paris VI, Paris.
- Gologanu, M., Leblond, J.-B., Devaux, J., 1993. Approximate models for ductile metals containing non-spherical voids — case of axisymmetric prolate ellipsoidal cavities. *Journal of the Mechanics and Physics of Solids* 41, 1723–1754.
- Gologanu, M., Leblond, J.-B., Devaux, J., 1994. Approximate models for ductile metals containing non-spherical voids — case of axisymmetric oblate ellipsoidal cavities. *Journal of Engineering Materials and Technology* 116, 290–297.
- Gologanu, M., Leblond, J.-B., Perrin, G., Devaux, J., 1995. Recent extensions of Gurson's model for porous ductile metals. In: Suquet, P. (Ed.) *Continuum Micromechanics*. Springer-Verlag.
- Gurson, A.L., 1977. Continuum theory of ductile rupture by void nucleation and growth, Part I — Yield criteria and flow rules for porous ductile media. *Journal of Engineering Materials and Technology* 99, 2–15.
- Hancock, J.W., Mackenzie, A.C., 1977. On the mechanisms of ductile failure in high-strength steels subjected to multi-axial stress-states. *Journal of the Mechanics and Physics of Solids* 14, 147–169.
- Hill, R., 1950. *The Mathematical Theory of Plasticity*. Clarendon Press, Oxford.
- Hom, C.L., McMeeking, R.M., 1989. Void growth in elastic-plastic materials. *Journal of Applied Mechanics* 56, 309–317.
- Huang, Y., 1991. Accurate dilatation rates for spherical voids in triaxial stress fields. *Journal of Applied Mechanics* 58, 1084–1085.
- Huang, Y., 1993. The role of non-uniform particle distribution in plastic flow localization. *Mechanics of Materials* 16, 265–279.
- Koplik, J., Needleman, A., 1988. Void growth and coalescence in porous plastic solids. *International Journal of Solids and Structures* 24, 835–853.
- Kuna, M., Sun, D.Z., 1996. Three-dimensional cell model analyses of void growth in ductile materials. *International Journal of Fracture* 81, 235–258.
- Leblond, J.-B., Perrin, G., 1999. A self-consistent approach to coalescence of cavities in inhomogeneously voided ductile solids. *Journal of the Mechanics and Physics of Solids* 47, 1823–1841.
- Leblond, J.-B., Perrin, G., Devaux, J., 1995. An improved Gurson-type model for hardenable ductile metals. *European Journal of Mechanics A/Solids* 14, 499–527.
- Lee, B.J., Mear, M.E., 1992. Axisymmetric deformations of power-law solids containing a dilute concentration of aligned spheroidal voids. *Journal of the Mechanics and Physics of Solids* 40, 1805–1836.
- Magnusen, P.E., Dubensky, E.M., Koss, D.A., 1988. The effect of void arrays on void linking during ductile fracture. *Acta Metallurgica* 36, 1503–1509.
- Magnusen, P.E., Srolovitz, D.J., Koss, D.A., 1990. A simulation of void linking during ductile microvoid fracture. *Acta Metallurgica et Materialia* 38, 1013–1022.
- Marini, B., Mudry, F., Pineau, A., 1985. Experimental study of cavity growth in ductile rupture. *Engineering Fracture Mechanics* 6, 989–996.
- McClintock, F.A., 1968a. A criterion for ductile fracture by the growth of holes. *Journal of Applied Mechanics* 35, 363–371.
- McClintock, F.A., 1968b. Local criteria for ductile fracture. *International Journal of Fracture* 4, 103–130.
- Mudry, F., Di Rienzo, F., Pineau, A., 1989. Numerical comparison of global and local fracture criteria in compact tension and center-crack panel specimens. In: Landes, J.D., Saxena, A., Merkle, J.G. (Eds.) *Non-Linear Fracture Mechanics: Volume II — Elastic-Plastic Fracture*. American Society for Testing and Materials, Philadelphia, pp. 24–39 (ASTM STP 995).
- Needleman, A., 1972. Void growth in an elastic-plastic medium. *Journal of Applied Mechanics* 39, 964–970.
- Needleman, A., Kushner, A.S., 1990. An analysis of void distribution effects on plastic flow in porous solids. *European Journal of Mechanics A/Solids* 9, 193–206.
- Needleman, A., Tvergaard, V., 1984. An analysis of ductile rupture in notched bars. *Journal of the Mechanics and Physics of Solids* 32, 461–490.

- Needleman, A., Tvergaard, V., 1987. An analysis of ductile rupture modes at a crack tip. *Journal of the Mechanics and Physics of Solids* 35, 151–183.
- Pardoen, T., Delannay, F., 1998a. Assessment of void growth models from porosity measurements in cold-drawn copper bars. *Metallurgical and Materials Transactions A* 29A, 1895–1908.
- Pardoen, T., Delannay, F., 1998b. The coalescence of voids in prestrained notched round copper bars. *Fatigue and Fracture of Engineering Materials and Structures* 21, 1459–1472.
- Pardoen, T., Doghri, I., Delannay, F., 1998. Experimental and numerical comparison of void growth models and void coalescence criteria for the prediction of ductile fracture in copper bars. *Acta Materialia* 46, 541–552.
- Perrin, G., Leblond, J.-B., 1990. Analytical study of a hollow sphere made of plastic porous material and subjected to hydrostatic tension — application to some problems in ductile fracture of metals. *International Journal of Plasticity* 6, 677–699.
- Pineau, A., 1992. Global and local approaches of fracture — transferability of laboratory test results to components. In: Argon, A.S. (Ed.) *Topics in Fracture and Fatigue*. Springer-Verlag, pp. 197–234.
- Ponte Castañeda, P., Zaidman, M., 1994. Constitutive models for porous materials with evolving microstructure. *Journal of the Mechanics and Physics of Solids* 42, 1459–1497.
- Richelsen, A.B., Tvergaard, V., 1994. Dilatant plasticity or upper bound estimates for porous ductile solids. *Acta Metallurgica et Materialia* 42, 2561–2577.
- Rogers, H.C., 1960. The tensile fracture of ductile metals. *Transactions of the Metallurgical Society of AIME* 218, 498–506.
- Rousselier, G., Devaux, J.-C., Mottet, G., Devesa, G., 1989. A methodology for ductile fracture analysis based on damage mechanics: an illustration of a local approach of fracture. In: Landes, J.D., Saxena, A., Merkle, J.G. (Eds.) *Nonlinear Fracture Mechanics: Volume II — Elastic-Plastic Fracture*. American Society for Testing and Materials, Philadelphia, pp. 332–354 (ASTM STP 995).
- Ruggieri, C., Panontin, T.L., Dodds, R.H. Jr., 1996. Numerical modeling of ductile crack growth in 3-D using computational cell elements. *International Journal of Fracture* 82, 67–95.
- Saje, M., Pan, J., Needleman, A., 1982. Void nucleation effects on shear localization in porous plastic solids. *International Journal of Fracture* 19, 163–182.
- Siruguet, K., 2000. Rupture ductile à basse triaxialité: effet des inclusions sur la croissance et la coalescence des cavités. Thèse de Doctorat de l'Université Paris VI, Paris.
- Sovik, O.P., Thaulow, C., 1997. Growth of spheroidal voids in elastic-plastic solids. *Fatigue and Fracture of Engineering Materials and Structures* 20, 1731–1744.
- Steglich, D., Brocks, W., 1997. Micromechanical modelling of the behaviour of ductile materials including particles. *Computational Materials Science* 9, 7–17.
- Thomason, P.F., 1985a. Three-dimensional models for the plastic limit-load at incipient failure of the intervoid matrix in ductile porous solids. *Acta Metallurgica* 33, 1079–1085.
- Thomason, P.F., 1985b. A three-dimensional model for ductile fracture by the growth and coalescence of microvoids. *Acta Metallurgica* 33, 1087–1095.
- Thomason, P.F., 1990. *Ductile Fracture of Metals*. Oxford, Pergamon Press.
- Thomason, P.F., 1993. Ductile fracture by the growth and coalescence of microvoids of non-uniform size and spacing. *Acta Metallurgica et Materialia* 41, 2127–2134.
- Thomson, C.I.A., Worswick, M.J., Pilkey, A.K., Lloyd, D.J., Burger, G., 1999. Modeling void nucleation and growth within periodic clusters of particles. *Journal of the Mechanics and Physics of Solids* 47, 1–26.
- Tvergaard, V., 1981. Influence of voids on shear band instabilities under plane strain conditions. *International Journal of Fracture* 17, 389–407.
- Tvergaard, V., 1982. On localization in ductile materials containing voids. *International Journal of Fracture* 18, 237–251.
- Tvergaard, V., 1990. Material failure by void growth to coalescence. *Advances in Applied Mechanics* 27, 83–151.
- Tvergaard, V., 1991. Failure by ductile cavity growth at a metal–ceramic interface. *Acta Metallurgica et Materialia* 39, 419–426.
- Tvergaard, V., 1997. Studies of void growth in a thin ductile layer between ceramics. *Computational Mechanics* 20, 186–191.

- Tvergaard, V., 1998. Interaction of very small voids with larger voids. *International Journal of Solids and Structures* 35, 3989–4000.
- Worswick, M.J., Pick, R.J., 1990. Void growth and constitutive softening in a periodically voided solid. *Journal of the Mechanics and Physics of Solids* 38, 601–625.
- Xia, L., Shih, C.F., 1995a. Ductile crack growth — I. A numerical study using computational cells with microstructurally-based length scales. *Journal of the Mechanics and Physics of Solids* 43, 233–259.
- Xia, L., Shih, C.F., 1995b. Ductile crack growth — II. Void nucleation and geometry effects on macroscopic fracture behaviour. *Journal of the Mechanics and Physics of Solids* 43, 1953–1981.
- Xia, L., Shih, C.F., Hutchinson, J.W., 1995. A computational approach to ductile crack growth under large scale yielding conditions. *Journal of the Mechanics and Physics of Solids* 43, 389–413.
- Zhang, Z.L., Niemi, E., 1995. A new failure criterion for the Gurson–Tvergaard dilational constitutive model. *International Journal of Fracture* 70, 321–334.